Cell Reports

Article

The hypoxia-regulated ectonucleotidase CD73 is a host determinant of HIV latency

Graphical abstract

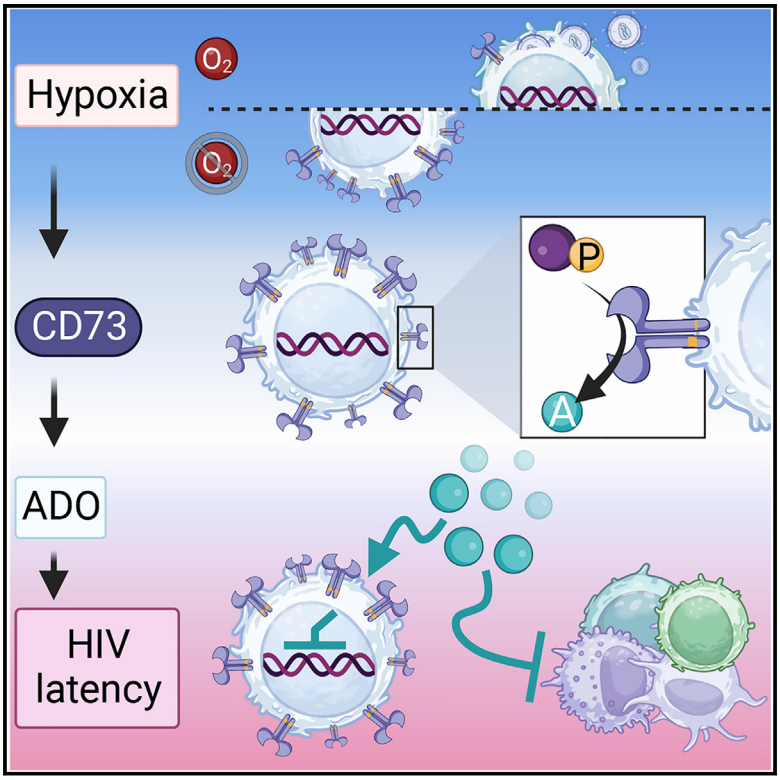

Authors

Hannah S. Sperber, Kyle A. Raymond, Mohamed S. Bouzidi, ..., Joachim Fandrey, Roland Schwarzer, Satish K. Pillai

Correspondence

roland-schwarzer@gmx.de (R.S.), satish.pillai@ucsf.edu (S.K.P.)

In brief

Using high-dimensional systems approaches, Sperber et al. show the role of CD73 in HIV infection and persistence. CD73, an immunosuppressive molecule, sustains dormant HIV in $CD4^+$ T cells by promoting transcriptional silencing and immune evasion. The described hypoxia-CD73-adenosine link underlying HIV persistence provides avenues for HIV-cure strategies.

Highlights

- CD73 surface expression is a key feature of HIV latently infected $CD4^+$ T cells
- Hypoxia enhances CD73 expression and promotes HIV persistence
- $CD73^+$ $CD4^+$ T cells harbor functional HIV reservoirs
- CD73-mediated adenosine signaling reinforces HIV latency

Sperber et al., 2023, Cell Reports *42*, 113285
November 28, 2023
https://doi.org/10.1016/j.celrep.2023.113285

CellPress

Cell Reports
Article

CellPress
OPEN ACCESS

Article

The hypoxia-regulated ectonucleotidase CD73 is a host determinant of HIV latency

Hannah S. Sperber,[1,2,3,6] Kyle A. Raymond,[1,3] Mohamed S. Bouzidi,[1,3] Tongcui Ma,[3,4] Silvana Valdebenito,[5] Eliseo A. Eugenin,[5] Nadia R. Roan,[3,4] Steven G. Deeks,[3] Sandra Winning,[7] Joachim Fandrey,[7] Roland Schwarzer,[6,*] and Satish K. Pillai[1,3,8,*]

[1]Vitalant Research Institute, San Francisco, CA, USA
[2]Free University of Berlin, Institute of Biochemistry, Berlin, Germany
[3]University of California, San Francisco, San Francisco, CA, USA
[4]Gladstone Institutes, San Francisco, CA, USA
[5]The University of Texas Medical Branch, Galveston, TX, USA
[6]University Hospital Essen, Institute for Translational HIV Research, Essen, Germany
[7]University of Duisburg-Essen, Institute for Physiology, Essen, Germany
[8]Lead contact
*Correspondence: roland-schwarzer@gmx.de (R.S.), satish.pillai@ucsf.edu (S.K.P.)
https://doi.org/10.1016/j.celrep.2023.113285

SUMMARY

Deciphering the mechanisms underlying viral persistence is critical to achieving a cure for human immunodeficiency virus (HIV) infection. Here, we implement a systems approach to discover molecular signatures of HIV latently infected CD4$^+$ T cells, identifying the immunosuppressive, adenosine-producing ectonucleotidase CD73 as a key surface marker of latent cells. Hypoxic conditioning, reflecting the lymphoid tissue microenvironment, increases the frequency of CD73$^+$ CD4$^+$ T cells and promotes HIV latency. Transcriptomic profiles of CD73$^+$ CD4$^+$ T cells favor viral quiescence, immune evasion, and cell survival. CD73$^+$ CD4$^+$ T cells are capable of harboring a functional HIV reservoir and reinitiating productive infection *ex vivo*. CD73 or adenosine receptor blockade facilitates latent HIV reactivation *in vitro*, mechanistically linking adenosine signaling to viral quiescence. Finally, tissue imaging of lymph nodes from HIV-infected individuals on antiretroviral therapy reveals spatial association between CD73 expression and HIV persistence *in vivo*. Our findings warrant development of HIV-cure strategies targeting the hypoxia-CD73-adenosine axis.

INTRODUCTION

In recent decades, remarkable scientific and biomedical advances have turned the tides in the ongoing fight against the global human immunodeficiency virus (HIV) epidemic. However, current therapeutic regimens fail to completely eradicate HIV due to the persistence of latently infected cells.[1] These viral reservoirs are established very early during infection, remain invisible to the host's immune system, and persevere for decades despite effective antiretroviral therapy (ART).[2–4] Although latently infected cells are extremely rare,[5–7] they are able to reinvigorate spreading infection rapidly, and people living with HIV (PLWH) almost inevitably experience viral rebound within weeks of a treatment interruption.[2,8]

The identification of reliable biomarkers or gene expression signatures in HIV latently infected cells is a key goal of current HIV research efforts. Such factors could contribute to the development of a cure by (1) refining and broadening our understanding of HIV latency mechanisms and the biology of viral persistence, (2) enabling accurate quantification of viral reservoirs to assess viral burden and efficacy of therapeutic interventions, and (3) providing potential therapeutic targets to specifically eliminate viral sanctuaries. However, the heterogeneous and dynamic nature of the viral reservoir greatly complicates this endeavor.[9]

Viral reservoirs are found in a variety of anatomical sites and cell types. Infected CD4$^+$ T cells arguably constitute the most important HIV reservoir,[10] and within this highly diverse cell lineage, the expression of several cellular factors is associated with increased levels of integrated proviral DNA.[11] This includes immune checkpoint molecules such as programmed cell death protein 1 (PD-1), cytotoxic T lymphocyte-associated protein 4 (CTLA-4), lymphocyte-activation gene 3 (LAG-3), and T cell immunoreceptor with immunoglobulin (Ig) and ITIM domains (TIGITs).[9,12,13] Moreover, expression levels of CD2 in CD4$^+$ T cells were reported to identify HIV latently infected cells,[14] while CD20[15]- and CD30[16]-expressing CD4$^+$ T cells were found to be specifically enriched for HIV RNA. In 2017, Descours et al.[17] proposed CD32a as a viral reservoir marker and described an unprecedented 1,000-fold enrichment in HIV-DNA in CD32a$^+$ cells as compared with CD32a$^-$ CD4$^+$ T cells. However, this finding has been repeatedly challenged in subsequent studies and has incited a controversial discussion.[18–25]

In the present study, we sought to provide a better understanding of the phenotypic nature of latently infected CD4$^+$

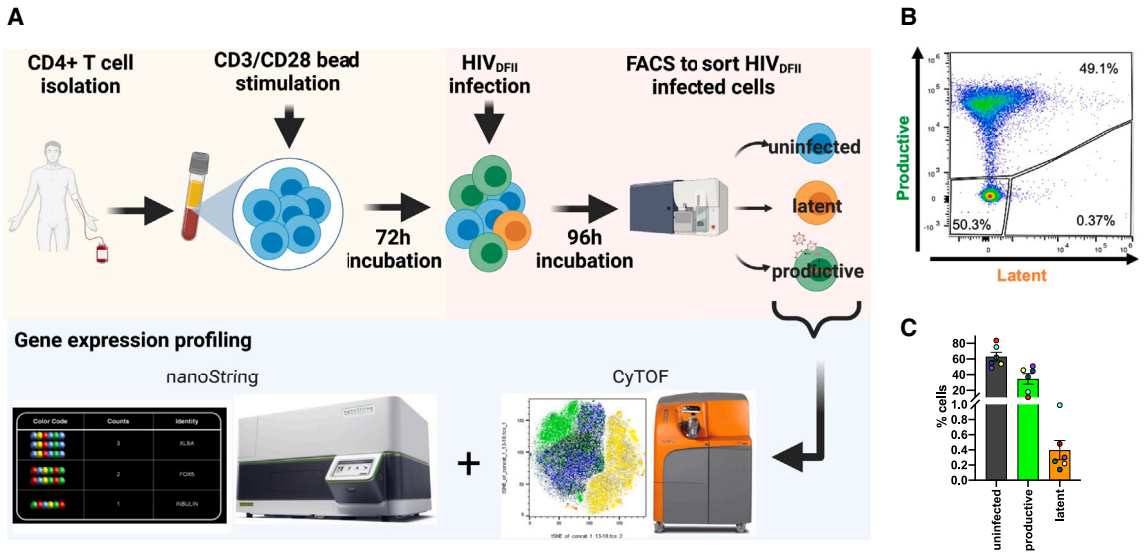

Figure 1. Isolation of latently infected primary CD4⁺ T cells using the dual-reporter virus HIV_{DFII}

(A) Experimental workflow: blood-derived primary CD4⁺ T cells were isolated from six healthy donors and stimulated *in vitro* with αCD3/αCD28 beads for 3 days. Cells were then infected with HIV_{DFII} and subjected to FACS 4 days post-infection.

(B) Representative gating for FACS of productively infected, latently infected, and uninfected CD4⁺ T cells. All samples were pregated for live, single cells.

(C) Bar graph represents the frequencies of infected cells in all six donors. Colored dots indicate individual donors. Error bars show standard error of the mean (SEM).

See also Figure S1.

T cells and the mechanisms involved in the establishment and maintenance of HIV reservoirs. To address this aim, we utilized a dual-reporter HIV construct that enables isolation and purification of uninfected, productively infected, and latently infected primary CD4⁺ T cells by flow cytometry.[26,27] We then characterized each of these purified cell populations using systems approaches to obtain comprehensive gene and protein expression profiles of HIV latently infected cells. Observed molecular signatures of latency were validated using *ex vivo* mechanistic experiments as well as profiling of tissue samples from HIV-infected individuals on suppressive ART. Our data reveal a mechanism of HIV latency establishment and maintenance, identifying the hypoxia-CD73-adenosine signaling axis as a key target for therapeutic intervention and diagnostic evaluation in the setting of HIV cure.

RESULTS

Sorting of HIV_{DFII}-infected primary CD4⁺ T cells enables isolation of latently infected cells

Profiling of HIV latently infected cells has been greatly impeded by their extremely low frequencies *in vivo* in HIV-infected individuals, as well as the lack of an established marker enabling purification of latent cells for downstream characterization. To characterize latent HIV reservoir cells, we utilized a modified version of the HIV Duo-Fluo I (HIV_{DFI}) single-round, recombinant HIV dual-reporter virus,[26,27] called HIV_{DFII} (Figure S1A). To achieve sufficient infection frequencies, we first activated blood-derived primary CD4⁺ T cells obtained from six healthy donors *in vitro* via αCD3/αCD28 bead stimulation and infected them with HIV_{DFII} via spinoculation (Figures S1B–S1D). Four days post-infection (p.i.), productively and latently infected, as well as uninfected, cells were purified by fluorescence-activated cell sorting (FACS; Figure 1A). Expectedly,[27] low frequencies of latently infected cells were established in all donors, whereas uninfected and productively infected cells could be rapidly collected by FACS in large numbers (Figures 1B and 1C). After testing the sorted samples for sufficient enrichment of the desired cell populations (Figure S1E), we subjected them, together with a panel of control specimens (untreated samples; unstimulated, infected cells; and stimulated cells without HIV_{DFII} infection), to downstream analysis using systems approaches (Figure 1A). All samples were characterized using mass cytometry by time of flight (CyTOF), measuring 40 surface proteins to provide immunophenotypic profiles at the single-cell level. In parallel, we applied NanoString hybridization and fluorescence-based digital counting technology, allowing for simultaneous detection of 770 mRNA and 30 protein targets.

Latently infected cells are phenotypically diverse and include Treg and Tfh cells

First, to establish an in-depth analysis of the phenotypic features of latently infected cells, we implemented CyTOF, simultaneously quantifying the expression levels of 40 different proteins with single-cell resolution. Our labeling panel comprised T cell lineage and differentiation markers, activation markers, homing receptors, and several proteins that were described previously in the context of HIV latency[9,28,29] (Table S1). We performed extensive high-dimensional analysis and generated t-distributed stochastic neighbor embedding (tSNE) plots to visualize the data

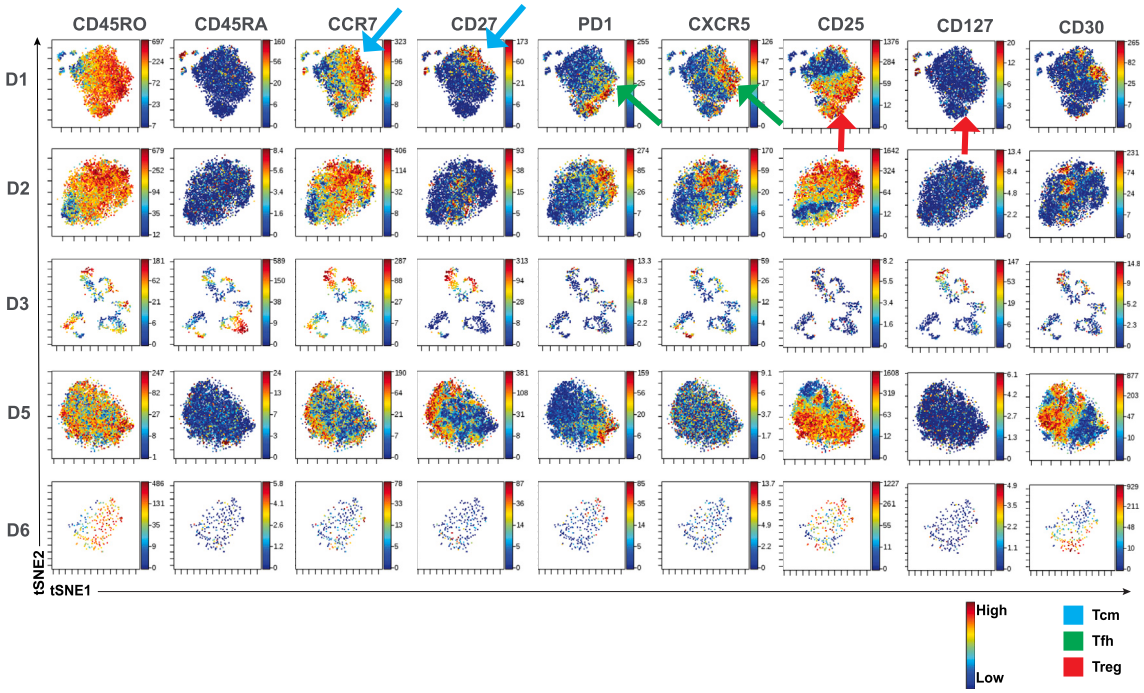

Figure 2. Multiple T cell subsets, including Treg cells, are represented among HIV latently infected cells

Shown are tSNE plots of CyTOF data describing sorted latent cells from each of 5 donors; each donor is analyzed within its own tSNE space (see also Figure S2). tSNEs are color-coded according to expression levels of the antigen listed at the top (with red corresponding to highest expression and blue the lowest). Most cells exhibited a memory phenotype, defined by high levels of CD45RO and low levels of CD45RA expression (first two columns). Latent cells exhibited phenotypic features of Tcm cells (CCR7$^+$ CD27$^+$), Tfh cells (PD1$^+$ CXCR5+), and Treg cells (CD25$^+$ CD127$^-$). Latent cells expressing CD30 (last column), a previously described marker of reservoir cells, were observed in all donors. Areas of the tSNE corresponding to these three cell subsets are highlighted by the blue, green, and red arrows, respectively, for D1.

and assess specific T cell subsets and population phenotypes. Cell clustering patterns in generated tSNE plots were largely driven by donor-dependent differences (Figure S2). Across all donors, we identified latent cells in various T cell compartments, including central memory (Tcm; CD45RO$^+$ CD45RA$^-$ CCR7$^+$ CD27$^+$), follicular helper (Tfh; CD45RO$^+$ CD45RA$^-$ PD1$^+$ CXCR5$^+$), regulatory (Treg; CD45RO$^+$ CD45RA$^-$ CD127$^-$ CD25$^+$), and, to a lesser extent, naive (CD45RO$^-$ CDRA$^+$ CCR7$^+$) T cells (Figure 2). Although memory CD4$^+$ T cell subset frequencies exhibited variability between donors and no significant associations with latency were identified, Treg cells were most commonly represented in latent cell populations. Interestingly, CD30, a previously reported marker of transcriptionally active reservoir cells,[16] was expressed on a subset of latent cells in all analyzed donors (Figure 2).

NanoString analysis reveals molecular features of latently infected cells that promote viral quiescence and cell survivorship

We next obtained high-dimensional NanoString data to comprehensively characterize gene and protein expression patterns of latent cells. Our initial unsupervised clustering analysis revealed that donor effects dominated expression patterns (Figure 3A, see dendrogram). Importantly, despite substantial donor effects, we observed that expression patterns in uninfected and productively infected cells within each donor clustered with respect to latent cells, suggesting that latently infected cells exhibited distinct expression signatures (Figure 3A, see dendrogram).

Expression data were then adjusted for confounding donor effects for downstream analyses. Subsequently, we examined changes in regulatory and signaling pathways in latent cells based on undirected and directed global significance scores (Figure 3B). The ‘‘antigen processing,’’ ‘‘adhesion,’’ ‘‘pathogen defense,’’ and ‘‘interleukins’’ pathways were the most significantly modulated pathways in the latent compartment. The upregulation of ‘‘interleukins’’ and ‘‘pathogen defense’’ in latently infected cells likely reflects intracellular signaling cascades that antagonize productive infection. The suppression of ‘‘antigen processing’’ in latent cells indicates the ability to evade host immunity, a prosurvival effect that could enforce viral persistence. This observation is in line with previous studies reporting that HIV actively subverts antigen presentation pathways.[30,31]

Next, overall target expression in the sorted samples was assessed by differential expression (DE) analysis (Figure 3C). Comparison of uninfected and latently infected cells revealed 16 differentially expressed targets (adjusted p value < 0.1), two of which were identified at the protein level: HLA-DRA protein was downregulated and NT5E (CD73) protein was upregulated on the surface of latent cells. DE analysis of productively and latently infected cells resulted in 36 significant hits (adjusted p value < 0.1), including cell surface CD4 protein and CD73 protein. CD4 protein was significantly downregulated in

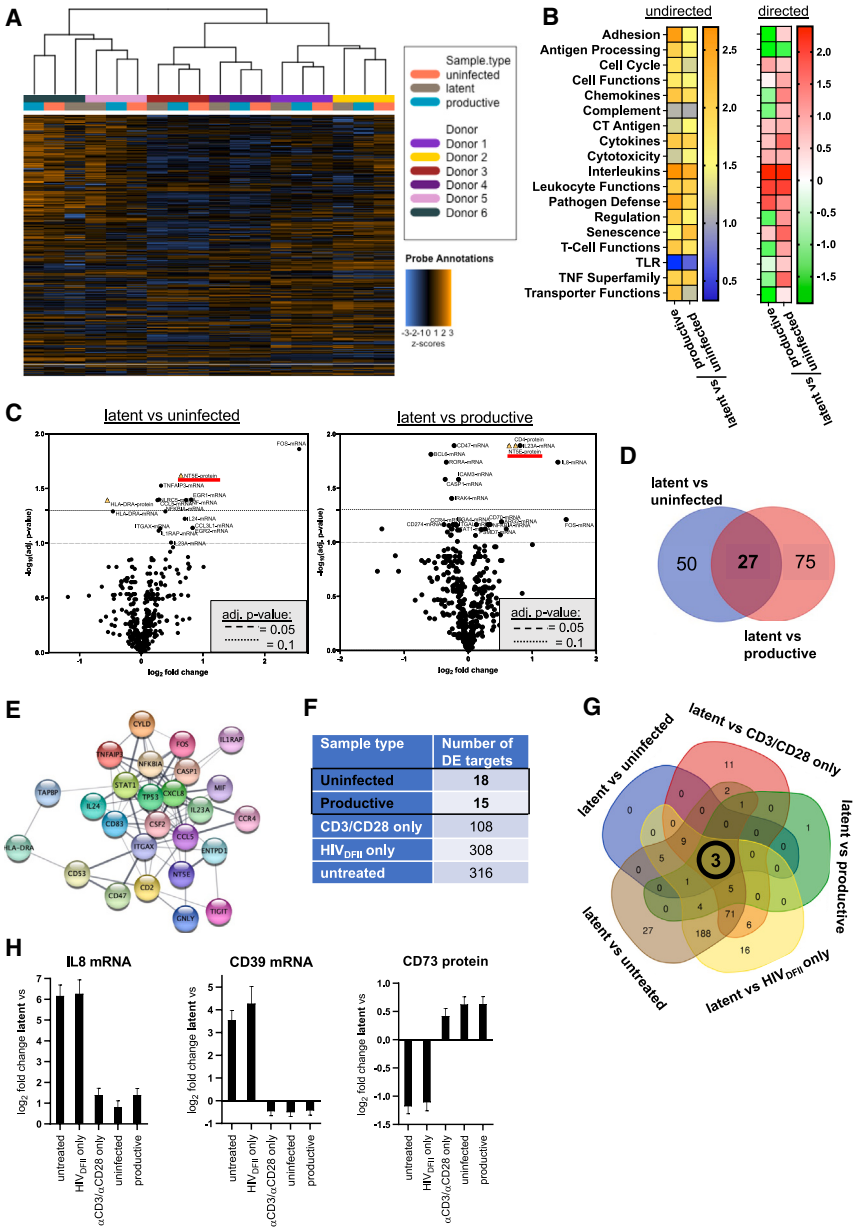

Figure 3. Latently infected cells share signature features including distinct expression of IL-8 mRNA, CD39 mRNA, and CD73 protein

(A) Heatmap visualizing normalized gene expression data from unsupervised clustering analysis of virus-exposed, sorted samples. Each row shows normalized counts of a single probe (target), and each column represents an individual sample. Colored horizontal bars along the top identify assigned sample attributes (donor or sample type, see color legend). Hierarchical clustering was used to generate dendrograms.

(B) Heatmaps showing undirected and directed global significance scores for signaling pathways based on differential gene expression analysis. The level of significance is indicated from blue to orange and the up- and downregulation of pathways from red to green.

(C) Volcano plots depict differential mRNA (circle) and protein (triangle) target expression between latent vs. uninfected and latent vs. productively infected cells. Each data point represents one target. The $\log_2$ fold change is displayed on the x axis, and the $-\log_{10}$ of the adjusted (adj.) p value (using the Benjamini-Hochberg method) is displayed on the y axis. Horizontal lines indicate adj. p value thresholds. The top 20 hits in each comparison are labeled. Hits were considered significant at an adj. p value cutoff <0.1. NT5E (CD73) is underlined in red.

(D) Venn diagram illustrating overlapping hits from the DE analyses latent vs. uninfected and latent vs. productive using a p value cutoff <0.05. Hits are listed in Table S2.

(E) A protein-protein interaction network of targets specifically changed in latent cells was generated in Cytoscape 3.8.2. The STRING database for *Homo sapiens* was applied with a confidence score of 0.4. Thickness of lines between nodes depicts confidence score, with a thicker line representing a higher score. HLA-DRB3 was not recognized by the software and thus was excluded from the interaction network.

(F) Number of differentially expressed genes from pairwise comparisons of latent cells to all other samples. Differential target expression between samples was performed with a p value cutoff <0.05.

(G) Venn diagram displaying the overlay of differential expression hits from comparisons of latently infected cells with all other samples using a p value cutoff <0.05.

(H) Bar graphs depict the $\log_2$ fold change of the indicated targets between latent cells and all other samples. Error bars show standard deviation (SD).

See also Figures S3 and S4.

productively infected cells (as expected in the setting of viral expression), and CD73 protein was again upregulated in latent cells.

Overlapping both individual DE analyses revealed 27 targets that were differentially modulated in latent infection ($p < 0.05$; Figure 3D) with respect to both productively infected and uninfected cells. These targets comprised CD2 mRNA, a checkpoint molecule that was reported previously as a surrogate marker for HIV reservoirs,[14] and, interestingly, CD73 as the only differentially expressed protein (Table S2). The list further included three mRNAs encoding transcription factors, six encoding cytokines, and 11 encoding surface proteins. Among these, *NFKBIA* (nuclear factor κB [NF-κB] inhibitor alpha) mRNA, which encodes a master inhibitor of the transcription factor NF-κB,[32] a crucial transcription factor of HIV,[33,34] was significantly upregulated in latent cells. In addition, *CASP1* mRNA was significantly downregulated in latently infected cells. CASP1 (caspase-1) is a key regulator of pyroptotic cell death, a highly inflammatory process that has been reported to be a major determinant of HIV pathogenesis and a potent driver of virus-dependent $CD4^+$ T cell depletion.[35]

The relationship between molecular markers of HIV latently infected cells was then investigated by utilizing the open-source software Cytoscape[36] to generate a detailed protein-protein

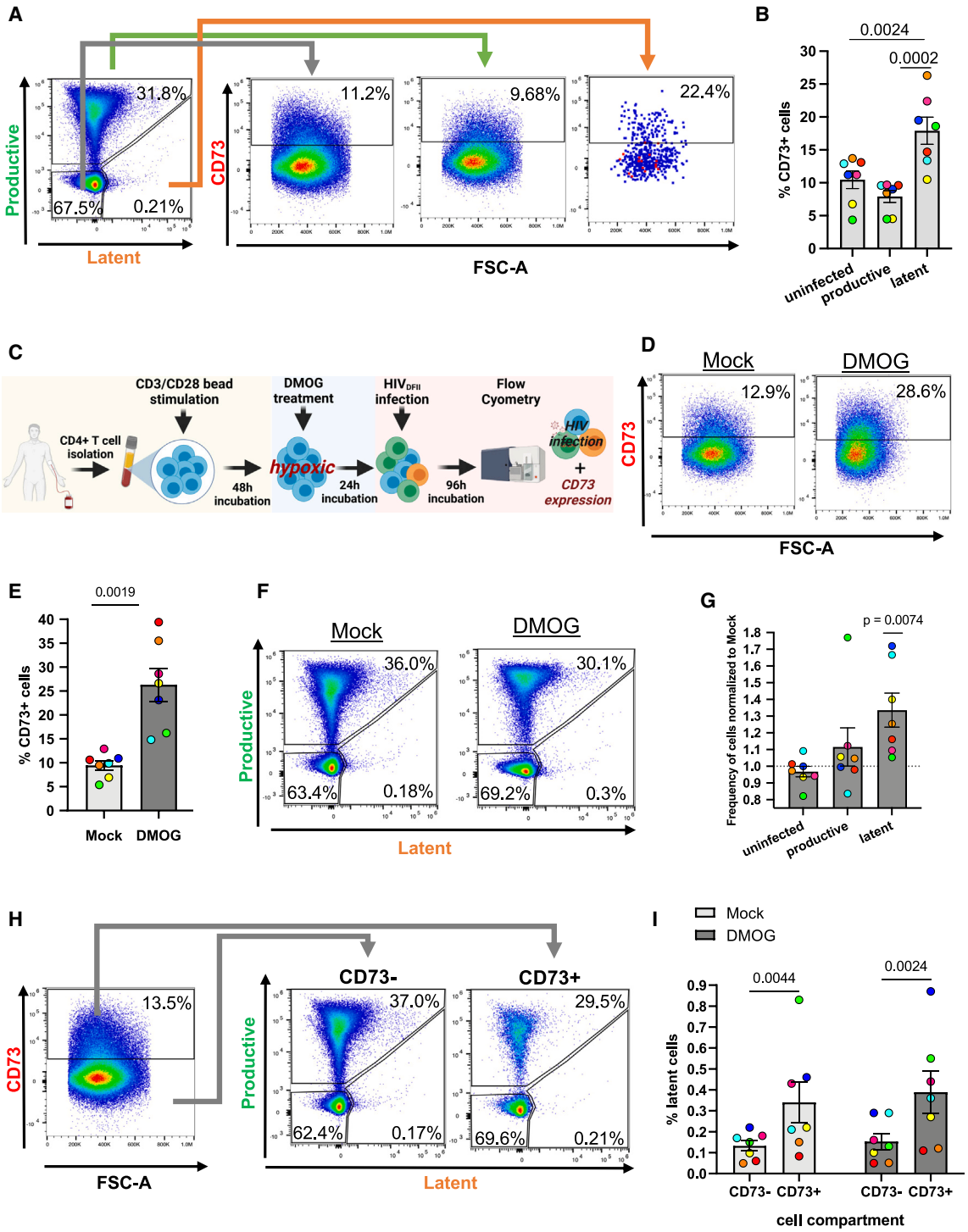

Figure 4. Hypoxic conditions increase the frequency of CD4$^+$ CD73$^+$ T cells and facilitate latent infection

(A) CD4$^+$ T cells from healthy individuals were infected with HIV$_{DFII}$ and analyzed by immunofluorescence staining and flow cytometry. Scatterplots show the gating strategy to analyze CD73 expression in HIV$_{DFII}$-infected cells from a single, representative donor.

(B) Shown is the frequency of CD73$^+$ cells in the respective HIV$_{DFII}$-infected cell population summarized from 7 donors. p values displayed above bars were generated by performing a one-way ANOVA with Tukey's multiple comparisons test.

(C) Experimental workflow for HIV$_{DFII}$ infection under hypoxic conditions.

(D and E) Representative flow plots of CD73 immunofluorescence staining in mock- or DMOG-treated CD4$^+$ T cells (D) and average frequency of CD73$^+$ CD4$^+$ T cells (E) across 7 donors. The p value was generated by performing a two-tailed paired t test.

(legend continued on next page)

interaction network (Figure 3E). Interestingly, all factors associated with HIV latency in our analyses were members of a single, established protein interaction complex. The chemotactic factor interleukin-8 (IL-8; or CXCL8) was found to have the highest number of immediate connections (17 first neighbors), followed by the transcription factor STAT1 (signal transducer and activator of transcription 1; 15 first neighbors) and the cytokine CSF2 (colony-stimulating factor 2; 15 first neighbors).

Three key members of the adenosinergic pathway, IL-8, CD39, and CD73, are differentially expressed in latent cells

To deepen our characterization of HIV latently infected cells, we additionally considered non-activated (no exposure to αCD3/αCD28-stimulating beads) and non-virus-exposed cell populations in our NanoString analyses. Inclusion of these comparators more faithfully emulates the *in vivo* landscape in ART-suppressed individuals where the majority of $CD4^+$ T cells are likely in a resting state and have not encountered HIV.

Next, DE analysis was implemented to compare latent cells in a pairwise fashion with all other cellular populations (Figure 3F). The pairwise DE analyses were then overlaid to identify genes that were differentially regulated in latently infected cells (Figure 3G). We identified three targets that were significantly modulated with respect to all other comparator groups: IL-8 mRNA, CD39 mRNA, and CD73 protein (a key marker revealed in our previous analyses) (Figure 3H). These three factors are known to be mechanistically connected through the adenosine signaling pathway, and our observed induction of IL-8 gene expression in latently infected cells (Figure 3H) potentially reflects ADORA2B stimulation.[37–41]

CD73 is highly expressed on a subset of PD-1+, CD39+, CD49d+, and $CD2^+$ cells

CD39 and CD73 are surface proteins and thus could serve as convenient indicators of latent reservoir cells. We therefore sought to examine correlations between the surface expression of CD73 and previously reported reservoir markers and enrichment factors, including CD2, CD49d, PD-1, CD39, CD98, CTLA-4, CD20, CD30, and CD32 in blood-derived $CD4^+$ T cells from PLWH. $CD4^+$ T cells were negatively selected from fresh blood collected from six PLWH on ART, and reservoir markers were measured by immunofluorescence staining and flow cytometry. Notably, none of the previously identified reservoir markers were enriched in the $CD73^+$ $CD4^+$ T cell compartment, and the frequency of PD-1 and CD39 expression was significantly reduced in $CD73^+$ cells as compared with total $CD4^+$ cell populations (Figures S3A and S3B). However, we also identified double-positive cells co-expressing high levels of CD73 and CD49d, CD2, PD-1, or CD39, respectively (Figure S3C, red arrows), indicating that these markers are not mutually exclusive *in vivo* in the setting of treated HIV infection. Expression levels of CD98, CTLA-4, CD20, CD30, and CD32 were extremely low in both total $CD4^+$ T and $CD73^+$ $CD4^+$ T cells (Figures S3B–S3D).

Based on unsupervised analyses including principal-component analysis (PCA), expression signatures were dominated by *in vitro* stimulation (Figures S4A and S4B). We therefore investigated T cell activation as a potential determinant of HIV latency by examining the expression levels of the established T cell surface markers CD45, CD45RO, and CD4 (Figure S4C), as well as panel-specific activation markers (Figures S4D and S4E). No significant associations were discovered between the expression levels of these activation markers and latent infection, suggesting that viral transcriptional fates are not dictated by cellular activation states.

Hypoxia promotes CD73 expression and HIV latency in primary $CD4^+$ T cells

To better understand the relevance of CD73 in the context of HIV infection and particularly in the establishment of the latent reservoir, we next focused on the regulation of CD73 expression.[42,43] Importantly, at least one hypoxia-response element (HRE) has been previously identified in the CD73 promoter region,[44] allowing for direct binding of hypoxia-inducible factors (HIFs). In this context, HIF-1 was demonstrated to control CD73 expression, with CD73 typically being upregulated under hypoxic conditions.[45] We therefore hypothesized that our discovery of CD73 upregulation in latent cells suggested that hypoxia may be the underlying cause of both increased CD73 expression and HIV latency.

We first confirmed our NanoString data using *in vitro* infection with HIV_{DFII} followed by immunofluorescence staining and flow cytometry, again observing a significant enrichment of $CD73^+$ cells among latently infected cells (Figures 4A and 4B). We then mimicked hypoxic conditions in our culture settings via administration of dimethyloxalylglycine (DMOG), followed by infection with HIV_{DFII} and flow cytometry (Figure 4C).

DMOG treatment substantially altered CD73 expression in $CD4^+$ T cells and led to a 2.5-fold increase of $CD73^+$ cells compared with mock treatment (Figures 4D and 4E). Similar levels of CD73 induction were observed in cells incubated at 1% oxygen, indicating that DMOG treatment accurately recapitulates the CD73 phenotype in $CD4^+$ T cells (Figure S5A). Notably, while CD73 expression was generally increased upon induction of hypoxic responses (compare Figures 4B and S5B), we observed a pronounced enrichment of $CD73^+$ cells specifically in the latent compartment, with up to 60% of latent cells being $CD73^+$ (Figure S5B). This was also reflected in CD73 expression

(F) Representative flow plots, showing HIV_{DFII} infection profiles 4 days post-HIV_{DFII} exposure upon mock or DMOG treatment.
(G) The frequency of DMOG-treated, HIV_{DFII}-infected cells was normalized to the respective mock population within each donor to account for donor variability. p values were generated by performing a two-way ANOVA with Fisher's least significant difference (LSD) test.
(H) Gating strategy used to analyze HIV_{DFII} infection profiles in the $CD4^+$ $CD73^{+/-}$ T cell compartments. Data shown are from a single, mock-treated donor and are representative for all seven donors.
(I) The average frequency of latently infected cells was assessed in $CD4^+$ $CD73^{+/-}$ T cells. Colored dots indicate individual donors. p values were generated by performing a two-way ANOVA with Fisher's LSD test. p value threshold for significance was at $p < 0.05$. Error bars show SEM.
See also Figure S5.

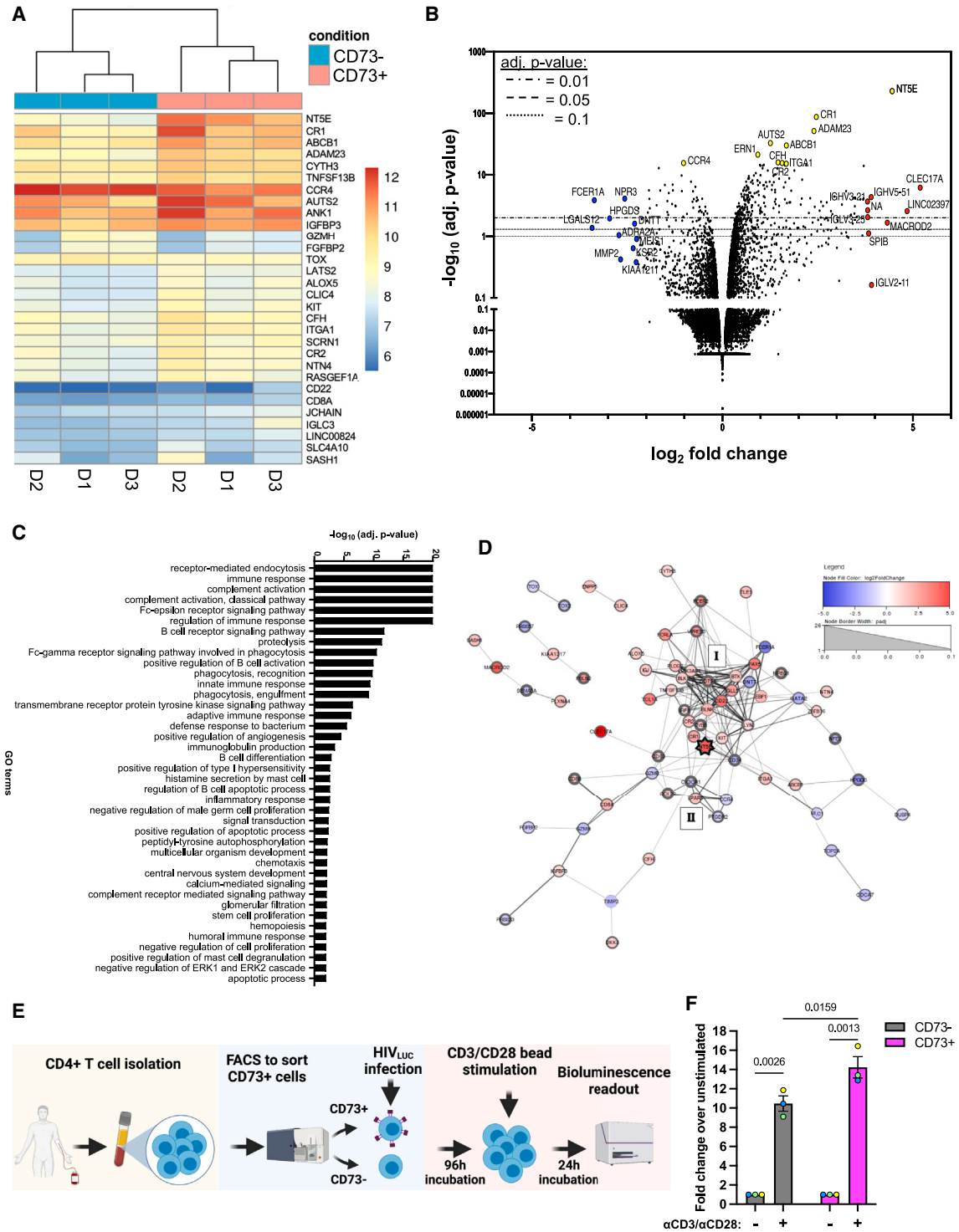

Figure 5. CD73$^+$ cells exhibit distinct immunoregulatory features and support HIV reactivation

(A) Clustering heatmap visualizing the expression profile of the top 30 differentially expressed genes sorted by their adjusted p value. Data were adjusted for donor effects.

(B) Global transcriptional changes between CD73$^-$ and CD73$^+$ cells are visualized in the volcano plot. Each data point represents a single gene. The $\log_2$ fold change of the normalized mean hit counts of each gene are plotted against $-\log_{10}$ of its adj. p value (using the Benjamini-Hochberg method). Horizontal lines indicate adj. p value thresholds. The top 10 most significantly changed (yellow), most upregulated (red), and most downregulated (blue) genes are highlighted.

(legend continued on next page)

per cell measured by mean fluorescence intensities (MFIs), which showed an overall increased CD73 expression in latent cells in both mock- and DMOG-treated samples (Figure S5C). Latent infection became significantly more abundant with a 33.6% increase upon DMOG treatment, while the frequency of uninfected or productive cells did not change significantly between culture conditions (Figures 4F and 4G).

Lastly, we examined whether CD73$^+$ cells were enriched for latent virus (Figure 4H). We measured a considerably higher rate of latently infected cells in CD73$^+$ compared with CD73$^-$ cells, with an average 3-fold enrichment of latent infection within the CD73$^+$ T cell compartment (Figure 4I). Considering the average frequency of CD73$^+$ cells among CD4$^+$ T cells (~10%; Figure 4E), these data suggest that approximately 25% of the overall, peripheral CD4$^+$ T cell HIV reservoir may reside in CD73$^+$ cells. Interestingly, the enrichment of latent cells in CD4$^+$ CD73$^+$ T cells did not significantly differ between mock- and DMOG-treated samples (Figure 4I), indicating that CD73$^+$ cells may possess specific features that favor the establishment and/or maintenance of latent infection that are not further modulated by the induction of hypoxic responses.

CD73$^+$ cells exhibit distinct immunoregulation and tyrosine kinase signaling

The role of CD73 in the context of oncogenesis, tumor progression, and survival is well described.[39] However, relatively little is known about the relevance and function of CD73 in human CD4$^+$ T cells. We thus characterized the transcriptome of blood-derived, primary CD73$^+$ and CD73$^-$ CD4$^+$ T cells by RNA sequencing. To address this aim, CD73$^{-/+}$ cells were isolated from primary CD4$^+$ T cells by FACS, revealing highly variable frequencies of CD73$^+$ CD4$^+$ T cells across donors, ranging from ~3% to ~23% (Figures S6A and S6B). Sorted cells were then subjected to RNA sequencing and DE analysis, accounting and adjusting for donor effects (Figures S6C and S6D). CD73$^-$ and CD73$^+$ CD4$^+$ T cells exhibited distinct transcriptional profiles and a clear clustering of the sorted populations (Figure 5A). Expectedly, CD73 (*NT5E*) exhibited highly significant divergence in expression levels between groups (Figure 5B). An additional 145 genes were differentially expressed, with 111 upregulated and 34 downregulated genes in CD73$^+$ cells (Figure 5B). *CR1*, *ADAM23*, *ABCB1*, and *AUTS2* were among the top genes upregulated in CD73$^+$ cells (Figure 5B, yellow dots). *CLEC17A* exhibited the highest fold change (>5-fold), followed by *CD73*, *LINC02397*, and *MACROD2* (>4-fold) (Figure 5B, red dots). Multiple genes were markedly downregulated in CD73$^+$ cells; however, only two of them reached the highest level of statistical significance (adjusted $p < 0.01$): *FCER1A* and *NPR3*. A gene set enrichment analysis yielded a multitude of significantly modulated pathways differentiating CD73$^+$ and CD73$^-$ cells including "immune responses," "complement activation," and "receptor-mediated signaling cascades" (Figure 5C), indicating diverging immunoregulatory programs. In addition, "positive regulation of angiogenesis," "regulation of apoptotic processes," and "tyrosine kinase signaling cascades" were among the 40 most significantly modulated pathways.

Next, all differentially expressed genes were uploaded into Cytoscape, and the resulting protein-protein interaction network was then overlaid with $\log_2$ fold changes and adjusted p values of each gene, visualizing directionality and significance of interacting hits (Figure 5D). The analysis revealed five distinct interaction networks, with one network containing the majority of hits. This approach revealed biological programs associated with the CD73$^+$ CD4$^+$ T cell compartment. Within this network, a tight cluster (I) of cell surface receptors was apparent (*CD22*, *CD79A*, *CR1*, *CR2*, *KIT*, *FCER1A*, *CD34*), accompanied by several signaling factors (*LYN*, *BLNK*, *BLK*, *BTK*, *PIK3AP1*, *TCL1A*) and transcription factors (*IRF8*, *EBF1*, *PAX5*). Another cluster (II) comprised downregulation of cell surface proteins *CXCR3*, *CCR4*, and *PTGDR2*. Importantly, the network also contained two significantly downregulated genes, transcription factor *GATA2* and DNA topoisomerase *TOP2A*, which are known to support active HIV transcription and replication.[46,47]

CD73$^+$ CD4$^+$ T cells harbor an inducible HIV reservoir

The intactness of integrated proviruses and the inducibility of viral gene expression are key attributes of the latent HIV reservoir. We therefore sought to investigate the capacity of CD73$^+$ T cells to harbor reactivatable latent virus. To this end, we adapted a primary *in vitro* HIV infection model[48] and infected FACS-sorted CD73$^-$ and CD73$^+$ CD4$^+$ T cells with the reporter virus HIV$_{Luc}$ (Figure 5E). After a resting period of 5 days, we stimulated cells with αCD3/αCD28 beads and observed a pronounced increase of viral transcription in both CD73$^-$ and CD73$^+$ CD4$^+$ T cells as compared with unstimulated cells, reflected by 10- and 14-fold increases in LTR-driven luciferase activity, respectively (Figure 5F). Induction of viral transcriptional activity was significantly higher in stimulated CD73$^+$ T cells as compared with CD73$^-$ T cells. These results demonstrate that the CD73$^+$ CD4$^+$ T cell compartment can harbor an inducible latent reservoir *in vitro*, indicating the potential of this compartment to contribute to spreading infection in PLWH upon treatment cessation.

Blocking the adenosine receptor A2AR or CD73 promotes HIV latency reversal

Bearing in mind the enzymatic function of CD73, we hypothesized that extracellular adenosine produced by CD73 could be

(C) Differentially expressed genes were grouped by their Gene Ontology (GO) and the enrichment of GO terms was tested using Fisher exact tests. The top 40 GO terms with an adj. p value <0.05 are displayed.

(D) The protein-protein interaction network of genes differentially expressed between CD73$^-$ and CD73$^+$ CD4$^+$ T cells was generated in Cytoscape as described previously. 33/145 hits were not recognized by the STRING database and thus were excluded from the interaction network. Among the remaining 112 genes, 43 genes did not have an interaction partner and are not displayed. $\log_2$ fold changes of genes are indicated by node pseudo color and the adj. p value by node border width. *CD73* (*NT5E*) is highlighted by a star shape. Protein clusters of interest are labeled.

(E) The schematic represents the experimental workflow to test reactivation of integrated provirus in sorted CD73$^-$ and CD73$^+$ CD4$^+$ T cells.

(F) Bars display the average fold change over unstimulated cells from three donors. Colored dots indicate individual donors. p values above bars were generated by performing a two-way ANOVA with Fisher's LSD. A p value at $p < 0.05$ was considered significant. Error bars show SEM.

See also Figure S6.

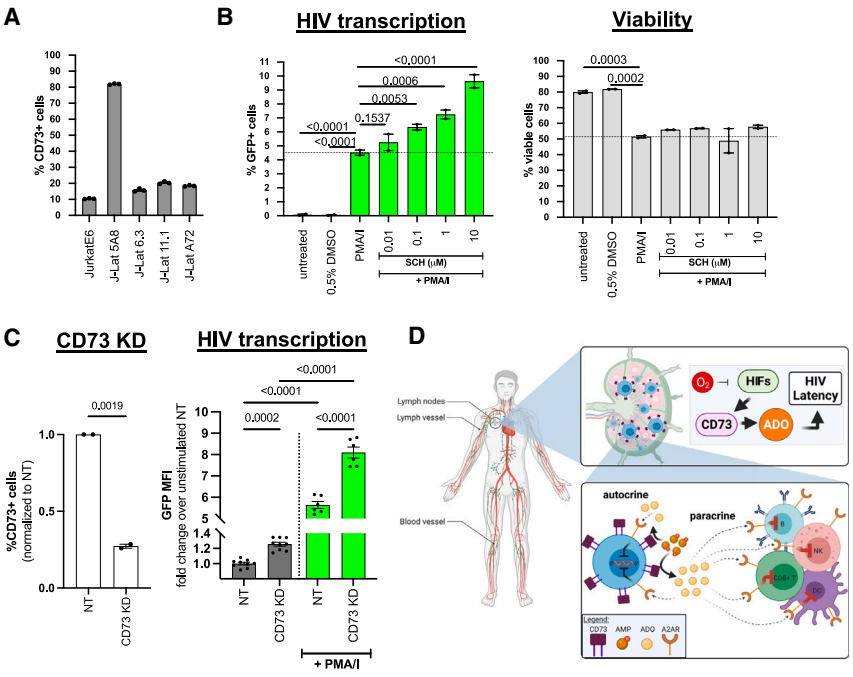

Figure 6. Blockade of CD73 and adenosine receptor A2AR facilitates HIV latency reversal

(A) Average frequency of live, single CD73$^+$ cells in the different T cell lines measured via flow cytometry.

(B) J-Lat 5A8 cells were treated with A2AR antagonist SCH-58261 (SCH) at indicated, increasing doses for 1 h, followed by treatment with PMA/I. PMA/I treatment alone served as positive control, and 0.5% DMSO treatment served as mock control. Cell viability based on forward scatter area (FSC-A) and side scatter area (SSC-A) and GFP expression as a reporter of HIV transcriptional activity was assessed 7 h post-treatment using flow cytometry. Samples were measured in duplicates. p values were generated by performing a one-way ANOVA with Fisher's LSD. p <0.05 was considered significant. Data represent the mean and error bars the SEM.

(C) J-Lat A72 cells were transduced with lentiviral vectors containing dCas9-KRAB sgRNAs targeting CD73 or a non-targeting (NT) control. CD73 KD was assessed via immunofluorescence staining of CD73 as measured by flow cytometry. Data were normalized to NT. Reactivation of viral transcription reflected by GFP expression was assessed by flow cytometry of A72 KD cells in the presence and the absence of PMA/I. Significance was determined by one-way ANOVA, comparing samples with NT.

(D) HCA model of HIV persistence. Under long-term ART, HIV persists *in vivo* preferentially in anatomical sanctuary sites like lymph nodes. Oxygen levels are known to be significantly lower in lymphoid tissues (0.5%–4.5%) compared with the in periphery (about 13%). Low oxygen supply or hypoxia leads to stabilization of hypoxia-inducible factors (HIFs), which control the expression of CD73. Upregulation of CD73 leads to the accumulation of adenosine (ADO) in the extracellular space. These factors favor the establishment of viral reservoirs and promote HIV persistence, silencing the provirus through autocrine signaling and inhibiting host antiviral immune responses by paracrine signaling mechanisms. T cells are shown in blue and CD73 in purple.

mechanistically involved in the establishment and/or maintenance of HIV latency. To test this, we investigated the adenosine signaling cascades downstream of CD73 in the well-established J-Lat cell line models of latency,[49,50] exploring how modulation of adenosine receptors by small-molecule drugs affects HIV transcriptional activity.

First, CD73 surface expression was measured in J-Lat clones, 5A8, 6.3, 11.1, and A72 as well as in the parental JurkatE6 cell line (Figure 6A). We found that between 10% and 20% of JurkatE6, J-Lat 6.3, 11.1, and A72 cells expressed CD73 on the surface, whereas about 80% of J-Lat 5A8 cells were CD73$^+$. In the next experiment, we sought to test whether an inhibition of adenosine signaling will impact HIV transcription in J-Lat cells. To that aim, J-Lat 5A8 cells were pretreated with the adenosine receptor antagonist SCH-58261 (SCH), followed by viral reactivation with PMA/I, a strong mitogen and latency-reversing agent. Notably, pretreatment with SCH significantly promoted latency reversal and resulted in an evident dose response with a 2-fold increase in the frequency of GFP$^+$ cells at the highest dose (Figure 6B). At the same time, SCH pretreatment did not compromise cell viability at any dose compared with cells treated with PMA/I only (Figure 6B).

Finally, we sought to determine if downregulation of CD73 itself affects HIV transcription and latency reversal. To pursue this objective, we performed CD73 knockdown (KD) via CRISPR interference (CRISPRi) in the A72 J-Lat clone. We first introduced the CRISPRi effector protein dCas9-KRAB by lentiviral transduction, generating the cell line J-Lat A72 CRISPRi. We then utilized another lentiviral vector to express single guide RNAs (sgRNAs) targeting CD73 or a non-targeting (NT) negative control, respectively. We tested KD efficiency by immunofluorescence staining of surface CD73, finding a significant downregulation of CD73 compared to NT controls (Figure 6C). CD73 KD resulted in significantly lower GFP expression levels in both stimulated and non-stimulated conditions (Figure 6C), indicating that CD73 exerts direct effects on HIV transcription and latency.

A comprehensive model of CD73-dependent latency

Based on our data obtained in *in vitro* infection models, we devised a model that incorporates hypoxia, CD73, and adenosine signaling, linking these factors with HIV transcriptional regulation and persistence. Our model predicts that the hypoxia-CD73-adenosine (HCA) axis plays a vital role, with CD73 as a central player in the maintenance of latent HIV infection (Figure 6D). As is known, HIV preferentially persists in lymphatic tissues,[51] which exhibit low oxygen levels and thus high levels of active HIFs. We surmise that the resulting upregulation of CD73 expression leads to adenosine-rich, immunosuppressive microenvironments, which promote the establishment and maintenance of latent reservoirs. Accumulation of extracellular adenosine thereby creates optimal conditions for HIV persistence by suppressing HIV host dependency factors through autocrine signaling cascades while impairing effective host immune responses through paracrine signaling mechanisms. Therefore, viral transcription is repressed, and immune escape

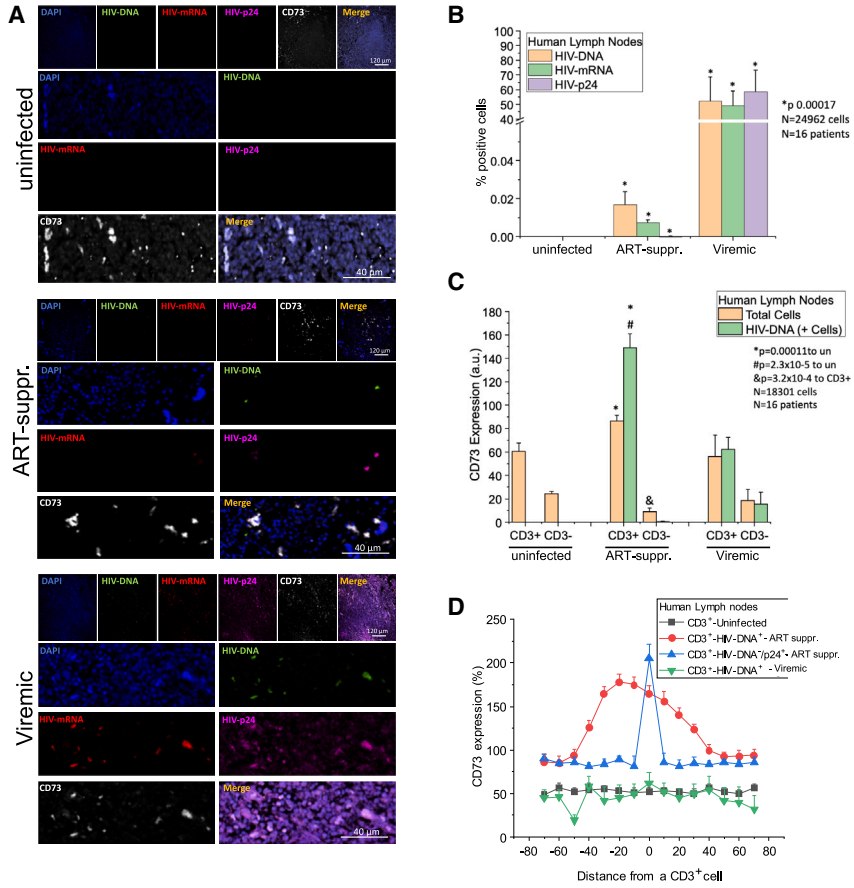

Figure 7. *In situ* imaging of lymph nodes from PLWH reveals associations between CD73 protein expression and HIV-DNA specifically in ART-suppressed individuals

(A) Representative confocal microscopy images for CD73 and HIV marker staining of lymph node tissue obtained from uninfected, ART-suppressed (suppr.), and viremic individuals.

(B) Automated image analysis of tissue sections stained for HIV-DNA, mRNA, and p24 protein in uninfected (n = 5), ART-suppr. (n = 6), and viremic individuals (n = 5). Bar graphs show the average percentage of cells that exhibit a positive signal for the respective target.

(C) Quantitative CD73 expression analysis in tissue samples from uninfected (n = 5), ART-suppr. (n = 6), and viremic individuals (n = 5). Identification of the T cell compartment ($CD3^+$ cells) and detection of HIV reservoir cells ($HIV\text{-}DNA^+$) was followed by quantification of CD73 signals in the indicated 4 cellular subsets ($CD3^+$ $HIV\text{-}DNA^-$, $CD3^+$ $HIV\text{-}DNA^+$, $CD3^-$ $HIV\text{-}DNA^-$, $CD3^-$ $HIV\text{-}DNA^+$). ANOVA was used to compare groups. Relevant statistics are shown in bar graphs.

(D) Quantification of CD73 expression and distribution in and around viral reservoirs in μM. Line plot analysis was performed as described in the STAR Methods and the schematic shown in Figure S7. 40–98 3D reconstructed images were analyzed per condition from 16 independent participant samples. CD73 intensity values were normalized to mean intensities in $CD3^+$ $HIV\text{-}DNA^-$/$p24^+$ ART suppr. samples.

of HIV-infected cells is facilitated, altogether promoting viral quiescence and survival of the latent reservoir.

Detection of HIV markers and CD73 *in vivo* in tissues from ART-suppressed HIV-infected individuals

To evaluate the clinical relevance of our findings and to test the HCA model *in vivo*, we applied a comprehensive tissue imaging pipeline that enables simultaneous detection of integrated HIV-DNA, viral mRNA, and HIV protein, as well as lineage markers, followed by quantitative image analyses.[52–54] We concomitantly detected CD73 expression and HIV markers in lymph node tissues (peripheral and inguinal lymph nodes) obtained from HIV-infected individuals on suppressive ART (ART suppr.), as well as in viremic untreated individuals and uninfected control subjects (Figure 7A). CD3 staining was used as a lineage marker for T cells, and DAPI was included as a counter stain of nuclear DNA. CD73 signals were found across all samples, while HIV detection expectedly differed greatly between ART-suppressed and viremic individuals and was absent in uninfected control samples (Figures 7A and 7B). Quantification of the viral reservoir in viremic individuals indicated that at least 40% of $CD3^+$ cells harbored integrated DNA and that most of these cells expressed viral RNA and HIV-p24 (Figure 7B, viremic). In contrast, in ART-suppressed individuals, 0.017% of $CD3^+$ cells contained viral DNA, half of which expressed viral RNA and 10% of which expressed viral proteins (Figure 7B, ART-suppr.).

CD73 expression correlates with HIV persistence in lymph nodes from ART-suppressed individuals

Next, we determined the association between HIV infection and CD73 expression, specifically in the $CD3^+$/$CD3^-$ cell compartment (Figure 7C). CD73 expression levels in $CD3^+$ cells were significantly higher in ART-suppressed samples than in uninfected samples. In addition, $HIV\text{-}DNA^+$ $CD3^+$ cells in ART-suppressed individuals exhibited a significant, 1.6-fold-higher CD73 expression compared with the overall $CD3^+$ population. This difference in CD73 expression levels was not observed in viremic individuals and suggested that CD73 expression may offer a survival advantage for HIV-infected cells in the setting of ART. We further hypothesized that viral reservoirs would not only reside in individual $CD73^+$ cells but rather also in CD73-rich, HIV-persistence-promoting microenvironments, due to local hypoxia and paracrine adenosine signaling effects. To explore this hypothesis, we performed imaging analysis by measuring the expression of CD73 in $CD3^+$/$HIV\text{-}DNA^+$ cells as well as neighboring uninfected cells surrounding viral reservoirs (Figures 7D and S7). Zero represents foci of viral infection, and increasing or decreasing distances correspond to neighboring uninfected cells (Figure 7D, up to 80 μm). Most localized

expression of CD73 was observed in and around viral reservoirs ($CD3^+$HIV-DNA) in ART-suppressed individuals. In addition, we observed that $CD3^+$ cells that were negative for HIV-DNA but HIV-$p24^+$ (HIV-$DNA^-/p24^+$), perhaps due to the uptake of viral particles, also had increased levels of CD73. In contrast, evenly distributed expression of CD73 was observed in uninfected and viremic lymph node tissues, confirming that the spatial association between CD73 expression and viral reservoirs is specific to ART-suppressed HIV infection (Figure 7D, black and green lines, respectively). Our data indicate that HIV-DNA^+ $CD3^+$ cells in lymph nodes from ART-suppressed individuals reside in areas with generally high CD73 expression, reinforcing that CD73, via adenosine production, contributes to HIV persistence (Figure 7D).

DISCUSSION

The latent HIV reservoir is considered to be the main obstacle to achieving viral eradication or indefinite disease remission in the absence of ART. It is generally believed that integrated provirus persists in specific cellular compartments and tissue sanctuaries, which enable both, long-term survival and spontaneous reactivation of viral replication even after decades of successful ART. The exact identity of the HIV reservoir, however, remains elusive. The goal of this study was to thoroughly characterize primary HIV latently infected cells using comprehensive and complementary systems approaches. Our work focused on $CD4^+$ T cells, the major target of HIV infection and an important potential source of viral rebound upon ART interruption.

The core finding of this work was the identification of elevated cell surface expression of CD73 as a signature characteristic of HIV latently infected $CD4^+$ T cells—an observation that, to the best of our knowledge, has not been described before. Using different *in vitro* models of HIV latency, we found indications that CD73 is not merely a passive marker of reservoir cells and that regulation of CD73 expression as well as its enzymatic function is mechanistically linked to HIV persistence.

Our NanoString analyses also revealed significant changes in the expression of CD39 and IL-8, which are mechanistically connected to CD73, within the latent compartment. In particular, the two ectonucleotidases CD39 and CD73 and their orchestrated functionality in purinergic signaling are well described in the literature.[39–41] In addition, IL-8 expression has been shown to be stimulated by adenosine signaling and is thus directly linked to the enzymatic function of CD73.[38] The distinctive expression of these three factors in latent cells suggests that CD73 and the adenosinergic pathway play pivotal roles in HIV latency and the establishment and/or maintenance of viral reservoirs.

Our initial *in vitro* infection model using HIV_{DFII} focused on a rather narrow time window of HIV latency, recapitulating the establishment and early persistence of viral reservoirs within a few days after infection. In the setting of HIV infection *in vivo*, HIV persists even after decades of fully suppressive ART. Linking the two observations, our *in situ* imaging of lymph node tissues demonstrated, for the first time, that a significant association between CD73 expression in T cells and HIV-DNA specifically in ART-suppressed individuals is maintained over extended periods of time. No spatial associations between CD73 and HIV markers were observed in tissues from viremic, untreated individuals. We surmise that in the absence of treatment, when HIV is not subject to pharmacologic selection pressure, active viral replication overrides CD73 effects and leads to rapid turnover of infected cells. In the setting of long-term ART, HIV-infected cells are subject to immune selection pressure, leading to an enrichment in $CD73^+$ infected cells due to their immunosuppressive nature and their increased likelihood of harboring transcriptionally inactive virus. This hypothesis is further reinforced by our transcriptomic profiling of blood-derived $CD73^+$ and $CD73^-$ $CD4^+$ T cell subsets, which revealed a spectrum of biological programs in the CD73 compartment that are expected to promote viral quiescence, immune evasion, and cell survivorship.

A key finding of our study is that CD73 is significantly upregulated under hypoxic conditions in the $CD4^+$ T cell compartment. This result is important for two reasons: (1) oxygen tension levels are highly variable throughout the body, ranging from 110 mmHg in well-oxygenated lung alveoli[55] down to 55–60 mmHg[56] in the gastrointestinal tract and 3–35 mmHg in lymphoid organs.[57,58] As a consequence, immune cells including $CD4^+$ T cells encounter and operate at varying oxygen concentrations as they traffic through the body.[58] Lymphoid organs, in particular, represent crucial viral sanctuaries, and as these are characterized by low oxygen levels, our data suggest a causal link between hypoxia, CD73 expression, and HIV persistence. (2) Hitherto, the roles of oxygen levels and hypoxia in HIV infection remained intangible and somewhat obscure. In 2009, Charles et al.[59] reported decreased HIV-1 RNA levels at 3% oxygen, while S. Deshmane and colleagues showed increased HIV transcription mediated by the interaction between HIV accessory protein Vpr and HIF-1α.[60,61] Moreover, HIV-1 replication was shown to be promoted by HIF-1α, which in turn was stabilized by reactive oxygen species.[62] Very recently, it was demonstrated that hypoxia can promote HIV latency with HIF-2α as a direct inhibitor of viral transcription.[63] Our data now provide insights into the connection between HIV latency and hypoxia, with CD73 emerging as key mediator bridging hypoxia and viral transcription.

As outlined above, our data suggest mechanistic involvement of CD73 in HIV persistence via its enzymatic function in the adenosine signaling cascade. Adenosine signaling leads to a suppression of cellular transcription factors that are critical for active viral transcription[64,65] and may create an ideal immunological niche for infected cells to evade host immune clearance due to an adenosine-mediated immunosuppressive microenvironment. Pharmacological blockade of A2AR in our latency model facilitated HIV latency reversal without impairing cell viability. Thus, our data demonstrate the potential of targeting the adenosinergic system as a therapeutic approach in the context of HIV infection and provide evidence that the enzymatic activity of CD73 is directly involved in HIV persistence. We would like to point out that hypoxia can regulate the expression of numerous genes,[66] including, but not limited to, CD39, the adenosine receptor ADORA2B, the equilibrium nucleoside transporter ENT-1, and

adenosine kinases (ADKs),[67] all of which could promote adenosine signaling independent of, or in concert with, CD73. Additional studies will therefore be necessary to determine how these diverse factors link hypoxia-mediated signaling to HIV persistence.

It is important to note that in recent years, increasing circumstantial evidence has been gathered independently, suggesting a critical role for either hypoxia,[59–63] CD73 expression,[68–70] or adenosine signaling[71–75] in HIV infection. Our findings reported here are complemented and validated by a recent translational study by Seddiki et al. demonstrating that HIV-infected CD73$^+$ memory CD4$^+$ T cells contribute significantly to the very long-lived HIV proviral DNA reservoir in treated individuals.[76] Our data now reveal a direct, causal connection that links the hypoxic regulation and adenosine-producing enzymatic activity of CD73 to the establishment and persistence of viral reservoirs.

Finally, the CD73-adenosine axis has received a great deal of attention in the context of cancer biology,[77–79] and the adenosinergic system has emerged as a promising new drug target in oncology.[38,39,80–85] Our data suggest that, like solid tumor cells, latent HIV reservoirs hijack the CD73-adenosine axis to subvert innate and adaptive immune responses, enhancing the survivorship of the infected cell as a persistence mechanism during ART. Therefore, CD73 and adenosine-focused anticancer therapeutics should be actively explored as foundations of HIV-cure approaches and host-directed therapies.

Limitations of the study

There are limitations to both our *in vivo* models and our *in vivo* profiling work that should be considered. Firstly, our *in vitro* HIV latency models are short-term infection models and were mainly geared at identifying host factors associated with the establishment of viral transcriptional latency in newly infected cells. These models do not capture the critical aspects of immunological selection that occur *in vivo* over the course of years or even decades of suppressive ART in PLWH; long-term selection pressures *in vivo* may result in enrichment of host factors on the surface of latently infected cells that do not appear in our *in vitro* profiling experiments. In regard to our *in vivo* profiling of lymphoid tissues, analyses of a much larger collection of tissue samples (from a broader array of anatomic sites associated with HIV persistence) will be required to fully appreciate the association between CD73 expression and the HIV reservoir. Moreover, our studies here have not considered HIV persistence outside of the lymphoid compartment; as there is evidence that myeloid lineage cells (e.g., monocyte-derived macrophages) harbor HIV, the relevance of adenosine signaling to HIV infection should be evaluated in these cell types as well. Lastly, although our *in vitro* experiments provide mechanistic connections between adenosine signaling and HIV persistence, much additional work remains to be done to decipher the relationship between adenosine signaling, HIV latency, and antiviral immunity *in vivo*. These future studies will be critical in guiding the development of HIV-cure strategies targeting the adenosine pathway.

STAR★METHODS

Detailed methods are provided in the online version of this paper and include the following:

- KEY RESOURCES TABLE
- RESOURCE AVAILABILITY
  - Lead contact
  - Materials availability
  - Data and code availability
- EXPERIMENTAL MODEL AND STUDY PARTICIPANT DETAILS
  - Bacterial strains
  - Cell lines
  - Study participants and primary CD4$^+$ T cell culture
  - Tissue samples
- METHOD DETAILS
  - Construction of next generation HIV_{DFII} reporter plasmid
  - Plasmid amplification and preparation
  - Virus production
  - Generation of CRISPRi cell lines
  - J-Lat cell latency reversal
  - CD4$^+$ T cell culture under hypoxic conditions
  - CD4$^+$ T cell *in vitro* infection
  - CD4$^+$ T cell *in vitro* infection and latency reversal
  - CD4$^+$ T cell staining and processing
  - Immunophenotyping of CD4$^+$ T cells from HIV-infected individuals
  - Flow cytometry gating and data analysis
  - Expression profiling via NanoString
  - CyTOF samples preparation and analysis
  - RNA sequencing
  - *In situ* detection of HIV and cellular markers in tissue samples
  - Image acquisition and analysis
- QUANTIFICATION AND STATISTICAL ANALYSIS

SUPPLEMENTAL INFORMATION

Supplemental information can be found online at https://doi.org/10.1016/j.celrep.2023.113285.

ACKNOWLEDGMENTS

The authors would like to acknowledge Guorui Xie, PhD, and Ashley George, PhD, for helpful input regarding the CyTOF analysis. The authors thank Leonard Chavez, PhD, and Shivani Desai for providing reagents and Vivienne Schneider for experimental support, as well as Konstantinos Georgiou, PhD, and Zain Y. Dossani, PhD, for guidance and support in data analysis. The authors sincerely thank Rebecca Hoh for her help in obtaining clinical specimens for our study.

This study was supported by National Institutes of Health (NIH) grants R01AI150449 and R01MH112457 (to S.K.P.). We would like to thank The National NeuroAIDS Tissue Consortium (NNTC) for providing all human samples and associated information. The NNTC is made possible through funding from the NIMH and NINDS by the following grants: Manhattan HIV Brain Bank (MHBB): U24MH100931; Texas NeuroAIDS Research Center (TNRC): U24MH100930; National Neurological AIDS Bank (NNAB): U24MH100929; California NeuroAIDS Tissue Network (CNTN): U24MH100928; and Data Coordinating Center (DCC): R01AI147777, R01AI127219, UM1AI64567, and

UM1AI64559. The staining and analysis were funded by National Institute of Mental Health grants MH096625 and MH128032 and the National Institute of Neurological Disorders and Stroke, NS105584 (to E.A.E.).

AUTHOR CONTRIBUTIONS

Conceptualization of the project, H.S.S., R.S., and S.K.P.; methodology, H.S.S. and R.S.; formal analysis, H.S.S., E.A.E., N.R.R., and R.S.; investigation, H.S.S., K.A.R., M.S.B., T.M., S.V., S.W., and R.S.; data curation, H.S.S., E.A.E., N.R.R., and R.S.; visualization, H.S.S., E.A.E., N.R.R., and R.S.; writing – original draft, H.S.S. and R.S.; writing – review & editing, H.S.S., K.A.R., M.S.B., E.A.E., N.R.R., S.W., J.F., R.S., and S.K.P.; supervision, R.S. and S.K.P.; resources, E.A.E., N.R.R., S.G.D., J.F., R.S., and S.K.P.; funding acquisition, E.A.E. and S.K.P.

DECLARATION OF INTERESTS

The authors declare no competing interests.

Received: November 15, 2022
Revised: July 4, 2023
Accepted: September 29, 2023
Published: October 31, 2023

REFERENCES

1. Ho, Y.-C., Shan, L., Hosmane, N.N., Wang, J., Laskey, S.B., Rosenbloom, D.I.S., Lai, J., Blankson, J.N., Siliciano, J.D., and Siliciano, R.F. (2013). Replication-Competent Noninduced Proviruses in the Latent Reservoir Increase Barrier to HIV-1 Cure. Cell *155*, 540–551. https://doi.org/10.1016/j.cell.2013.09.020.
2. Davey, R.T., Bhat, N., Yoder, C., Chun, T.W., Metcalf, J.A., Dewar, R., Natarajan, V., Lempicki, R.A., Adelsberger, J.W., Miller, K.D., et al. (1999). HIV-1 and T cell dynamics after interruption of highly active antiretroviral therapy (HAART) in patients with a history of sustained viral suppression. Proc. Natl. Acad. Sci. USA *96*, 15109–15114. https://doi.org/10.1073/pnas.96.26.15109.
3. Finzi, D., Blankson, J., Siliciano, J.D., Margolick, J.B., Chadwick, K., Pierson, T., Smith, K., Lisziewicz, J., Lori, F., Flexner, C., et al. (1999). Latent infection of CD4+ T cells provides a mechanism for lifelong persistence of HIV-1, even in patients on effective combination therapy. Nat. Med. *5*, 512–517. https://doi.org/10.1038/8394.
4. Siliciano, J.D., and Siliciano, R.F. (2000). Latency and viral persistence in HIV-1 infection. J. Clin. Invest. *106*, 823–825. https://doi.org/10.1172/JCI11246.
5. Chun, T.W., Carruth, L., Finzi, D., Shen, X., DiGiuseppe, J.A., Taylor, H., Hermankova, M., Chadwick, K., Margolick, J., Quinn, T.C., et al. (1997). Quantification of latent tissue reservoirs and total body viral load in HIV-1 infection. Nature *387*, 183–188. https://doi.org/10.1038/387183a0.
6. Finzi, D., Hermankova, M., Pierson, T., Carruth, L.M., Buck, C., Chaisson, R.E., Quinn, T.C., Chadwick, K., Margolick, J., Brookmeyer, R., et al. (1997). Identification of a reservoir for HIV-1 in patients on highly active antiretroviral therapy. Science *278*, 1295–1300. https://doi.org/10.1126/science.278.5341.1295.
7. Wong, J.K., Hezareh, M., Günthard, H.F., Havlir, D.V., Ignacio, C.C., Spina, C.A., and Richman, D.D. (1997). Recovery of replication-competent HIV despite prolonged suppression of plasma viremia. Science *278*, 1291–1295. https://doi.org/10.1126/science.278.5341.1291.
8. Strategies for Management of Antiretroviral Therapy SMART Study Group; El-Sadr, W.M., Lundgren, J.D., Neaton, J.D., Gordin, F., Abrams, D., Arduino, R.C., Babiker, A., Burman, W., Clumeck, N., et al. (2006). CD4+ Count–Guided Interruption of Antiretroviral Treatment. N. Engl. J. Med. *355*, 2283–2296. https://doi.org/10.1056/nejmoa062360.
9. Neidleman, J., Luo, X., Frouard, J., Xie, G., Hsiao, F., Ma, T., Morcilla, V., Lee, A., Telwatte, S., Thomas, R., et al. (2020). Phenotypic analysis of the unstimulated in vivo hiv cd4 t cell reservoir. Elife *9*, e60933. https://doi.org/10.7554/ELIFE.60933.
10. Kulpa, D.A., and Chomont, N. (2015). HIV persistence in the setting of antiretroviral therapy: when, where and how does HIV hide? J. Virus Erad. *1*, 59–66.
11. Darcis, G., Berkhout, B., and Pasternak, A.O. (2019). The quest for cellular markers of HIV reservoirs: Any color you like. Front. Immunol. *10*, 2251. https://doi.org/10.3389/fimmu.2019.02251.
12. Fromentin, R., Bakeman, W., Lawani, M.B., Khoury, G., Hartogensis, W., DaFonseca, S., Killian, M., Epling, L., Hoh, R., Sinclair, E., et al. (2016). CD4+ T Cells Expressing PD-1, TIGIT and LAG-3 Contribute to HIV Persistence during ART. PLoS Pathog. *12*, e1005761. https://doi.org/10.1371/journal.ppat.1005761.
13. McGary, C.S., Deleage, C., Harper, J., Micci, L., Ribeiro, S.P., Paganini, S., Kuri-Cervantes, L., Benne, C., Ryan, E.S., Balderas, R., et al. (2017). CTLA-4+PD-1− Memory CD4+ T Cells Critically Contribute to Viral Persistence in Antiretroviral Therapy-Suppressed, SIV-Infected Rhesus Macaques. Immunity *47*, 776–788.e5. https://doi.org/10.1016/j.immuni.2017.09.018.
14. Iglesias-Ussel, M., Vandergeeten, C., Marchionni, L., Chomont, N., and Romerio, F. (2013). High Levels of CD2 Expression Identify HIV-1 Latently Infected Resting Memory CD4+ T Cells in Virally Suppressed Subjects. J. Virol. *87*, 9148–9158. https://doi.org/10.1128/jvi.01297-13.
15. Serra-Peinado, C., Grau-Expósito, J., Luque-Ballesteros, L., Astorga-Gamaza, A., Navarro, J., Gallego-Rodriguez, J., Martin, M., Curran, A., Burgos, J., Ribera, E., et al. (2019). Expression of CD20 after viral reactivation renders HIV-reservoir cells susceptible to Rituximab. Nat. Commun. *10*, 1–15. https://doi.org/10.1038/s41467-019-11556-4.
16. Hogan, L.E., Vasquez, J., Hobbs, K.S., Hanhauser, E., Aguilar-Rodriguez, B., Hussien, R., Thanh, C., Gibson, E.A., Carvidi, A.B., Smith, L.C.B., et al. (2018). Increased HIV-1 transcriptional activity and infectious burden in peripheral blood and gut-associated CD4+ T cells expressing CD30. PLoS Pathog. *14*, e1006856. https://doi.org/10.1371/journal.ppat.1006856.
17. Descours, B., Petitjean, G., López-Zaragoza, J.L., Bruel, T., Raffel, R., Psomas, C., Reynes, J., Lacabaratz, C., Levy, Y., Schwartz, O., et al. (2017). CD32a is a marker of a CD4 T-cell HIV reservoir harbouring replication-competent proviruses. Nature *543*, 564–567. https://doi.org/10.1038/nature21710.
18. Pérez, L., Anderson, J., Chipman, J., Thorkelson, A., Chun, T.W., Moir, S., Haase, A.T., Douek, D.C., Schacker, T.W., and Boritz, E.A. (2018). Conflicting evidence for HIV enrichment in CD32+ CD4 T cells. Nature *561*, E9–E16. https://doi.org/10.1038/s41586-018-0493-4.
19. Osuna, C.E., Lim, S.Y., Kublin, J.L., Apps, R., Chen, E., Mota, T.M., Huang, S.H., Ren, Y., Bachtel, N.D., Tsibris, A.M., et al. (2018). Evidence that CD32a does not mark the HIV-1 latent reservoir. Nature *561*, E20–E28. https://doi.org/10.1038/s41586-018-0495-2.
20. Martin, G.E., Pace, M., Thornhill, J.P., Phetsouphanh, C., Meyerowitz, J., Gossez, M., Brown, H., Olejniczak, N., Lwanga, J., Ramjee, G., et al. (2018). CD32-expressing CD4 T cells are phenotypically diverse and can contain proviral HIV DNA. Front. Immunol. *9*, 928. https://doi.org/10.3389/fimmu.2018.00928.
21. Thornhill, J.P., Pace, M., Martin, G.E., Hoare, J., Peake, S., Herrera, C., Phetsouphanh, C., Meyerowitz, J., Hopkins, E., Brown, H., et al. (2019). CD32 expressing doublets in HIV-infected gut-associated lymphoid tissue are associated with a T follicular helper cell phenotype. Mucosal Immunol. *12*, 1212–1219. https://doi.org/10.1038/s41385-019-0180-2.
22. Noto, A., Procopio, F.A., Banga, R., Suffiotti, M., Corpataux, J.-M., Cavassini, M., Riva, A., Fenwick, C., Gottardo, R., Perreau, M., and Pantaleo, G. (2018). CD32 + and PD-1 + Lymph Node CD4 T Cells Support Persistent HIV-1 Transcription in Treated Aviremic Individuals. J. Virol. *92*, e00901-18–e00919. https://doi.org/10.1128/jvi.00901-18.
23. Vásquez, J.J., Aguilar-Rodriguez, B.L., Rodriguez, L., Hogan, L.E., Somsouk, M., McCune, J.M., Deeks, S.G., Laszik, Z.G., Hunt, P.W., and

Henrich, T.J. (2019). CD32-RNA Co-localizes with HIV-RNA in CD3+ Cells Found within Gut Tissues from Viremic and ART-Suppressed Individuals. Pathog. Immun. *4*, 147–160. https://doi.org/10.20411/pai.v4i1.271.

24. Adams, P., Fievez, V., Schober, R., Amand, M., Iserentant, G., Rutsaert, S., Dessilly, G., Vanham, G., Hedin, F., Cosma, A., et al. (2021). CD32+CD4+ memory T cells are enriched for total HIV-1 DNA in tissues from humanized mice. iScience *24*, 101881. https://doi.org/10.1016/J.ISCI.2020.101881.

25. Darcis, G., Kootstra, N.A., Hooibrink, B., van Montfort, T., Maurer, I., Groen, K., Jurriaans, S., Bakker, M., van Lint, C., Berkhout, B., and Pasternak, A.O. (2020). CD32+CD4+ T Cells Are Highly Enriched for HIV DNA and Can Support Transcriptional Latency. Cell Rep. *30*, 2284–2296.e3. https://doi.org/10.1016/J.CELREP.2020.01.071.

26. Calvanese, V., Chavez, L., Laurent, T., Ding, S., and Verdin, E. (2013). Dual-color HIV reporters trace a population of latently infected cells and enable their purification. Virology *446*, 283–292. https://doi.org/10.1016/j.virol.2013.07.037.

27. Chavez, L., Calvanese, V., and Verdin, E. (2015). HIV Latency Is Established Directly and Early in Both Resting and Activated Primary CD4 T Cells. PLoS Pathog. *11*, e1004955. https://doi.org/10.1371/journal.ppat.1004955.

28. Ma, T., Luo, X., George, A.F., Mukherjee, G., Sen, N., Spitzer, T.L., Giudice, L.C., Greene, W.C., and Roan, N.R. (2020). HIV efficiently infects T cells from the endometrium and remodels them to promote systemic viral spread. Elife *9*, e55487-24. https://doi.org/10.7554/ELIFE.55487.

29. Xie, G., Luo, X., Ma, T., Frouard, J., Neidleman, J., Hoh, R., Deeks, S.G., Greene, W.C., and Roan, N.R. (2021). Characterization of HIV-induced remodeling reveals differences in infection susceptibility of memory CD4 + T cell subsets in vivo. Cell Rep. *35*, 109038. https://doi.org/10.1016/J.CELREP.2021.109038.

30. Kerkau, T., Gernert, S., Kneitz, C., and Schimpl, A. (1992). Mechanism of MHC Class I Downregulation in HIV Infected Cells. Immunobiology *184*, 402–409. https://doi.org/10.1016/S0171-2985(11)80597-8.

31. Cohen, G.B., Gandhi, R.T., Davis, D.M., Mandelboim, O., Chen, B.K., Strominger, J.L., and Baltimore, D. (1999). The selective downregulation of class I major histocompatibility complex proteins by HIV-1 protects HIV-infected cells from NK cells. Immunity *10*, 661–671. https://doi.org/10.1016/S1074-7613(00)80065-5.

32. Jacobs, M.D., and Harrison, S.C. (1998). Structure of an IκBα/NF-κB complex. Cell *95*, 749–758. https://doi.org/10.1016/S0092-8674(00)81698-0.

33. Ruelas, D.S., and Greene, W.C. (2013). An Integrated Overview of HIV-1 Latency. Cell *155*, 519–529. https://doi.org/10.1016/j.cell.2013.09.044.

34. Greene, W.C., and Peterlin, B.M. (2002). Charting HIV's remarkable voyage through the cell: Basic science as a passport to future therapy. Nat. Med. *8*, 673–680. https://doi.org/10.1038/nm0702-673.

35. Doitsh, G., Galloway, N.L.K., Geng, X., Yang, Z., Monroe, K.M., Zepeda, O., Hunt, P.W., Hatano, H., Sowinski, S., Muñoz-Arias, I., and Greene, W.C. (2014). Cell death by pyroptosis drives CD4 T-cell depletion in HIV-1 infection. Nature *505*, 509–514. https://doi.org/10.1038/nature12940.

36. Otasek, D., Morris, J.H., Bouças, J., Pico, A.R., and Demchak, B. (2019). Cytoscape Automation: empowering workflow-based network analysis. Genome Biol. *20*, 185. https://doi.org/10.1186/s13059-019-1758-4.

37. Allard, B., Allard, D., Buisseret, L., and Stagg, J. (2020). The adenosine pathway in immuno-oncology. Nat. Rev. Clin. Oncol. *17*, 611–629. https://doi.org/10.1038/s41571-020-0382-2.

38. Kazemi, M.H., Raoofi Mohseni, S., Hojjat-Farsangi, M., Anvari, E., Ghalamfarsa, G., Mohammadi, H., and Jadidi-Niaragh, F. (2018). Adenosine and adenosine receptors in the immunopathogenesis and treatment of cancer. J. Cell. Physiol. *233*, 2032–2057. https://doi.org/10.1002/jcp.25873.

39. Di Virgilio, F., and Adinolfi, E. (2017). Extracellular purines, purinergic receptors and tumor growth. Oncogene *36*, 293–303. https://doi.org/10.1038/onc.2016.206.

40. Yegutkin, G.G., Henttinen, T., Samburski, S.S., Spychala, J., and Jalkanen, S. (2002). The evidence for two opposite, ATP-generating and ATP-consuming, extracellular pathways on endothelial and lymphoid cells. Biochem. J. *367*, 121–128.

41. Antonioli, L., Pacher, P., Vizi, E.S., and Haskó, G. (2013). CD39 and CD73 in immunity and inflammation. Trends Mol. Med. *19*, 355–367. https://doi.org/10.1016/j.molmed.2013.03.005.

42. Hansen, K.R., Resta, R., Webb, C.F., and Thompson, L.F. (1995). Isolation and characterization of the promoter of the human 5′-nucleotidase (CD73)-encoding gene. Gene *167*, 307–312. https://doi.org/10.1016/0378-1119(95)00574-9.

43. Fausther, M., Sheung, N., Saiman, Y., Bansal, M.B., and Dranoff, J.A. (2012). Activated hepatic stellate cells upregulate transcription of ecto-5=-nucleotidase/CD73 via specific SP1 and SMAD promoter elements. Am. J. Physiol. Gastrointest. Liver Physiol. *303*, 904–914. https://doi.org/10.1152/ajpgi.00015.2012.-Adeno.

44. Synnestvedt, K., Furuta, G.T., Comerford, K.M., Louis, N., Karhausen, J., Eltzschig, H.K., Hansen, K.R., Thompson, L.F., and Colgan, S.P. (2002). Ecto-5′-nucleotidase (CD73) regulation by hypoxia-inducible factor-1 mediates permeability changes in intestinal epithelia. J. Clin. Invest. *110*, 993–1002. https://doi.org/10.1172/JCI200215337.

45. Kordaß, T., Osen, W., and Eichmüller, S.B. (2018). Controlling the immune suppressor: Transcription factors and MicroRNAs regulating CD73/NT5E. Front. Immunol. *9*, 813. https://doi.org/10.3389/fimmu.2018.00813.

46. Towatari, M., Kanei, Y., Saito, H., and Hamaguchi, M. (1998). Hematopoietic transcription factor GATA-2 activates transcription from HIV-1 long terminal repeat. AIDS *12*, 253–259. https://doi.org/10.1097/00002030-199803000-00002.

47. Lokeswara Balakrishna, S., Satyanarayana, N., and Kondapi, A.K. (2013). Involvement of human topoisomerase II isoforms in HIV-1 reverse transcription. Arch. Biochem. Biophys. *532*, 91–102. https://doi.org/10.1016/j.abb.2013.01.010.

48. Lassen, K.G., Hebbeler, A.M., Bhattacharyya, D., Lobritz, M.A., and Greene, W.C. (2012). A Flexible Model of HIV-1 Latency Permitting Evaluation of Many Primary CD4 T-Cell Reservoirs. PLoS One *7*, e30176. https://doi.org/10.1371/journal.pone.0030176.

49. Jordan, A., Bisgrove, D., and Verdin, E. (2003). HIV reproducibly establishes a latent infection after acute infection of T cells in vitro. EMBO J. *22*, 1868–1877. https://doi.org/10.1093/emboj/cdg188.

50. Chan, J.K., Bhattacharyya, D., Lassen, K.G., Ruelas, D., and Greene, W.C. (2013). Calcium/Calcineurin Synergizes with Prostratin to Promote NF-κB Dependent Activation of Latent HIV. PLoS One *8*, e77749. https://doi.org/10.1371/journal.pone.0077749.

51. Lamers, S.L., Rose, R., Maidji, E., Agsalda-Garcia, M., Nolan, D.J., Fogel, G.B., Salemi, M., Garcia, D.L., Bracci, P., Yong, W., et al. (2016). HIV DNA Is Frequently Present within Pathologic Tissues Evaluated at Autopsy from Combined Antiretroviral Therapy-Treated Patients with Undetectable Viral Loads. J. Virol. *90*, 8968–8983. https://doi.org/10.1128/jvi.00674-16.

52. Prevedel, L., Ruel, N., Castellano, P., Smith, C., Malik, S., Villeux, C., Bomsel, M., Morgello, S., and Eugenin, E.A. (2019). Identification, Localization, and Quantification of HIV Reservoirs Using Microscopy. Curr. Protoc. Cell Biol. *82*, 64. https://doi.org/10.1002/cpcb.64.

53. Donoso, M., D'amico, D., Valdebenito, S., Hernandez, C.A., Prideaux, B., and Eugenin, E.A. (2022). Identification, Quantification, and Characterization of HIV-1 Reservoirs in the Human Brain. https://doi.org/10.3390/cells11152379.

54. D'Amico, D., Barone, R., Di Felice, V., Ances, B., Prideaux, B., and Eugenin, E.A. (2023). Chronic brain damage in HIV-infected individuals under antiretroviral therapy is associated with viral reservoirs, sulfatide release,

and compromised cell-to-cell communication. Cell. Mol. Life Sci. *80*, 116. https://doi.org/10.1007/s00018-023-04757-0.

55. Carreau, A., El Hafny-Rahbi, B., Matejuk, A., Grillon, C., and Kieda, C. (2011). Why is the partial oxygen pressure of human tissues a crucial parameter? Small molecules and hypoxia. J. Cell Mol. Med. *15*, 1239–1253. https://doi.org/10.1111/j.1582-4934.2011.01258.x.

56. Zenewicz, L.A. (2017). Oxygen Levels and Immunological Studies. Front. Immunol. *8*, 324. https://doi.org/10.3389/fimmu.2017.00324.

57. Caldwell, C.C., Kojima, H., Lukashev, D., Armstrong, J., Farber, M., Apasov, S.G., and Sitkovsky, M.V. (2001). Differential Effects of Physiologically Relevant Hypoxic Conditions on T Lymphocyte Development and Effector Functions. J. Immunol. *167*, 6140–6149. https://doi.org/10.4049/jimmunol.167.11.6140.

58. Ohta, A., Diwanji, R., Kini, R., Subramanian, M., Ohta, A., and Sitkovsky, M. (2011). In vivo T cell activation in lymphoid tissues is inhibited in the oxygen-poor microenvironment. Front. Immunol. *2*, 27. https://doi.org/10.3389/fimmu.2011.00027.

59. Charles, S., Ammosova, T., Cardenas, J., Foster, A., Rotimi, J., Jerebtsova, M., Ayodeji, A.A., Niu, X., Ray, P.E., Gordeuk, V.R., et al. (2009). Regulation of HIV-1 transcription at 3% versus 21% oxygen concentration. J. Cell. Physiol. *221*, 469–479. https://doi.org/10.1002/jcp.21882.

60. Deshmane, S.L., Amini, S., Sen, S., Khalili, K., and Sawaya, B.E. (2011). Regulation of the HIV-1 promoter by HIF-1α and Vpr proteins. Virol. J. *8*, 477. https://doi.org/10.1186/1743-422X-8-477.

61. Deshmane, S.L., Mukerjee, R., Fan, S., Del Valle, L., Michiels, C., Sweet, T., Rom, I., Khalili, K., Rappaport, J., Amini, S., and Sawaya, B.E. (2009). Activation of the Oxidative Stress Pathway by HIV-1 Vpr Leads to Induction of Hypoxia-inducible Factor 1α Expression. J. Biol. Chem. *284*, 11364–11373. https://doi.org/10.1074/jbc.M809266200.

62. Duette, G., Gerber, P.P., Rubione, J., Perez, P.S., Landay, A.L., Crowe, S.M., Liao, Z., Witwer, K.W., Holgado, M.P., Salido, J., et al. (2018). Induction of HIF-1α by HIV-1 Infection in CD4 + T Cells Promotes Viral Replication and Drives Extracellular Vesicle-Mediated Inflammation. mBio *9*, 1–21. https://doi.org/10.1128/mBio.00757-18.

63. Zhuang, X., Pedroza-pacheco, I., Nawroth, I., Kliszczak, A.E., Magri, A., Paes, W., Rubio, C.O., Yang, H., Ashcroft, M., Mole, D., et al. (2020). Hypoxic microenvironment shapes HIV-1 replication and latency. Commun. Biol. *3*, 376. https://doi.org/10.1038/s42003-020-1103-1.

64. Romio, M., Reinbeck, B., Bongardt, S., Hüls, S., Burghoff, S., and Schrader, J. (2011). Extracellular purine metabolism and signaling of CD73-derived adenosine in murine Treg and Teff cells. Am. J. Physiol. Cell Physiol. *301*, C530–C539. https://doi.org/10.1152/ajpcell.00385.2010.

65. Sheridan, C.M., Heist, E.K., Beals, C.R., Crabtree, G.R., and Gardner, P. (2002). Protein kinase A negatively modulates the nuclear accumulation of NF-ATc1 by priming for subsequent phosphorylation by glycogen synthase kinase-3. J. Biol. Chem. *277*, 48664–48676. https://doi.org/10.1074/jbc.M207029200.

66. D'Alessandro, S., Magnavacca, A., Perego, F., Fumagalli, M., Sangiovanni, E., Prato, M., Dell'Agli, M., and Basilico, N. (2019). Effect of Hypoxia on Gene Expression in Cell Populations Involved in Wound Healing. BioMed Res. Int. *2019*, 2626374–2626420. https://doi.org/10.1155/2019/2626374.

67. Poth, J.M., Brodsky, K., Ehrentraut, H., Grenz, A., and Eltzschig, H.K. (2013). Transcriptional control of adenosine signaling by hypoxia-inducible transcription factors during ischemic or inflammatory disease. J. Mol. Med. *91*, 183–193. https://doi.org/10.1007/s00109-012-0988-7.

68. Tóth, I., Le, A.Q., Hartjen, P., Thomssen, A., Matzat, V., Lehmann, C., Scheurich, C., Beisel, C., Busch, P., Degen, O., et al. (2013). Decreased frequency of CD73 + CD8 + T cells of HIV-infected patients correlates with immune activation and T cell exhaustion. J. Leukoc. Biol. *94*, 551–561. https://doi.org/10.1189/jlb.0113018.

69. Schuler, P.J., Macatangay, B.J.C., Saze, Z., Jackson, E.K., Riddler, S.A., Buchanan, W.G., Hilldorfer, B.B., Mellors, J.W., Whiteside, T.L., and Rinaldo, C.R. (2013). CD4+CD73+ T cells are associated with lower T-cell activation and C reactive protein levels and are depleted in HIV-1 infection regardless of viral suppression. AIDS *27*, 1545–1555. https://doi.org/10.1097/QAD.0b013e328360c7f3.

70. Wang, X., Zhang, L., Du, J., Wei, Y., Wang, D., Song, C., Chen, D., Li, B., Jiang, M., Zhang, M., et al. (2022). Decreased CD73+ Double-Negative T Cells and Elevated Level of Soluble CD73 Correlated With and Predicted Poor Immune Reconstitution in HIV-Infected Patients After Antiretroviral Therapy. Front. Immunol. *13*, 869286. https://doi.org/10.3389/FIMMU.2022.869286.

71. Li, J., Huang, H.H., Tu, B., Zhou, M.J., Hu, W., Fu, Y.L., Li, X.Y., Yang, T., Song, J.W., Fan, X., et al. (2021). Reversal of the CD8+ T-Cell Exhaustion Induced by Chronic HIV-1 Infection Through Combined Blockade of the Adenosine and PD-1 Pathways. Front. Immunol. *12*, 687296–687311. https://doi.org/10.3389/fimmu.2021.687296.

72. Nikolova, M., Carriere, M., Jenabian, M.A., Limou, S., Younas, M., Kök, A., Huë, S., Seddiki, N., Hulin, A., Delaneau, O., et al. (2011). CD39/Adenosine Pathway Is Involved in AIDS Progression. PLoS Pathog. *7*, e1002110. https://doi.org/10.1371/journal.ppat.1002110.

73. He, T., Brocca-Cofano, E., Gillespie, D.G., Xu, C., Stock, J.L., Ma, D., Policicchio, B.B., Raehtz, K.D., Rinaldo, C.R., Apetrei, C., et al. (2015). Critical Role for the Adenosine Pathway in Controlling Simian Immunodeficiency Virus-Related Immune Activation and Inflammation in Gut Mucosal Tissues. J. Virol. *89*, 9616–9630. https://doi.org/10.1128/jvi.01196-15.

74. Moreno-Fernandez, M.E., Rueda, C.M., Rusie, L.K., and Chougnet, C.A. (2011). Regulatory T cells control HIV replication in activated T cells through a cAMP-dependent mechanism. Blood *117*, 5372–5380. https://doi.org/10.1182/blood-2010-12-323162.

75. Li, G., Nunoya, J.I., Cheng, L., Reszka-Blanco, N., Tsao, L.C., Jeffrey, J., and Su, L. (2017). Regulatory T Cells Contribute to HIV-1 Reservoir Persistence in CD4 + T Cells Through Cyclic Adenosine Monophosphate-Dependent Mechanisms in Humanized Mice in Vivo. J. Infect. Dis. *216*, 1579–1591. https://doi.org/10.1093/infdis/jix547.

76. Seddiki, N., Zaunders, J., Phetsouphanh, C., Brezar, V., Xu, Y., Mcguire, H.M., Bailey, M., Mcbride, K., Hey-Cunningham, W., Mee, C., et al. (2021). CD73 + CD127 high Long-Term Memory CD4 T Cells Are Highly Proliferative in Response to Recall Antigens and Are Early Targets in HIV-1 Infection. Int. J. Mol. Sci. *22*, 912. https://doi.org/10.3390/ijms22020912.

77. Zhang, B. (2012). CD73 promotes tumor growth and metastasis. Oncolmmunology *1*, 67–70. https://doi.org/10.4161/onci.1.1.18068.

78. Chen, S., Fan, J., Zhang, M., Qin, L., Dominguez, D., Long, A., Wang, G., Ma, R., Li, H., Zhang, Y., et al. (2019). CD73 expression on effector T cells sustained by TGF-β facilitates tumor resistance to anti-4-1BB/CD137 therapy. Nat. Commun. *10*, 150–215. https://doi.org/10.1038/s41467-018-08123-8.

79. Vijayan, D., Barkauskas, D.S., Stannard, K., Sult, E., Buonpane, R., Takeda, K., Teng, M.W.L., Sachsenmeier, K., Hay, C., and Smyth, M.J. (2017). Selective activation of anti-CD73 mechanisms in control of primary tumors and metastases. OncoImmunology *6*, e1312044. https://doi.org/10.1080/2162402X.2017.1312044.

80. Allard, D., Chrobak, P., Allard, B., Messaoudi, N., and Stagg, J. (2019). Targeting the CD73-adenosine axis in immuno-oncology. Immunol. Lett. *205*, 31–39. https://doi.org/10.1016/j.imlet.2018.05.001.

81. Sek, K., Mølck, C., Stewart, G.D., Kats, L., Darcy, P.K., and Beavis, P.A. (2018). Targeting Adenosine Receptor Signaling in Cancer Immunotherapy. Int. J. Mol. Sci. *19*, 3837. https://doi.org/10.3390/ijms19123837.

82. Leone, R.D., and Emens, L.A. (2018). Targeting adenosine for cancer immunotherapy. J. Immunother. Cancer *6*, 57. https://doi.org/10.1186/s40425-018-0360-8.

83. Chen, S., Wainwright, D.A., Wu, J.D., Wan, Y., Matei, D.E., Zhang, Y., and Zhang, B. (2019). CD73: an emerging checkpoint for cancer

immunotherapy. Immunotherapy *11*, 983–997. https://doi.org/10.2217/imt-2018-0200.

84. Antonioli, L., Yegutkin, G.G., Pacher, P., Blandizzi, C., and Haskó, G. (2016). Anti-CD73 in Cancer Immunotherapy: Awakening New Opportunities. Trends Cancer *2*, 95–109. https://doi.org/10.1016/j.trecan.2016.01.003.

85. Zhang, B. (2010). CD73: A Novel Target for Cancer Immunotherapy. Cancer Res. *70*, 6407–6411. https://doi.org/10.1158/0008-5472.CAN-10-1544.

86. Spina, C.A., Anderson, J., Archin, N.M., Bosque, A., Chan, J., Famiglietti, M., Greene, W.C., Kashuba, A., Lewin, S.R., Margolis, D.M., et al. (2013). An In-Depth Comparison of Latent HIV-1 Reactivation in Multiple Cell Model Systems and Resting CD4+ T Cells from Aviremic Patients. PLoS Pathog. *9*, e1003834. https://doi.org/10.1371/journal.ppat.1003834.

87. Sakaue-Sawano, A., Kurokawa, H., Morimura, T., Hanyu, A., Hama, H., Osawa, H., Kashiwagi, S., Fukami, K., Miyata, T., Miyoshi, H., et al. (2008). Visualizing spatiotemporal dynamics of multicellular cell-cycle progression. Cell *132*, 487–498. https://doi.org/10.1016/j.cell.2007.12.033.

88. Ho, S.-M., Hartley, B.J., Flaherty, E., Rajarajan, P., Abdelaal, R., Obiorah, I., Barretto, N., Muhammad, H., Phatnani, H.P., Akbarian, S., and Brennand, K.J. (2017). Evaluating Synthetic Activation and Repression of Neuropsychiatric-Related Genes in hiPSC-Derived NPCs, Neurons, and Astrocytes. Stem Cell Rep. *9*, 615–628. https://doi.org/10.1016/j.stemcr.2017.06.012.

89. Heckl, D., Kowalczyk, M.S., Yudovich, D., Belizaire, R., Puram, R.V., McConkey, M.E., Thielke, A., Aster, J.C., Regev, A., and Ebert, B.L. (2014). Generation of mouse models of myeloid malignancy with combinatorial genetic lesions using CRISPR-Cas9 genome editing. Nat. Biotechnol. *32*, 941–946. https://doi.org/10.1038/nbt.2951.

90. Gent, U. of Draw Venn Diagram. Bioinforma. Evol. Genet. http://bioinformatics.psb.ugent.be/webtools/Venn/.

91. Bolger, A.M., Lohse, M., and Usadel, B. (2014). Trimmomatic: a flexible trimmer for Illumina sequence data. Bioinformatics *30*, 2114–2120. https://doi.org/10.1093/bioinformatics/btu170.

92. Dobin, A., Davis, C.A., Schlesinger, F., Drenkow, J., Zaleski, C., Jha, S., Batut, P., Chaisson, M., and Gingeras, T.R. (2013). STAR: ultrafast universal RNA-seq aligner. Bioinforma. Oxf. Engl. *29*, 15–21. https://doi.org/10.1093/bioinformatics/bts635.

93. Love, M.I., Huber, W., and Anders, S. (2014). Moderated estimation of fold change and dispersion for RNA-seq data with DESeq2. Genome Biol. *15*, 550. https://doi.org/10.1186/s13059-014-0550-8.

94. Berg, S., Kutra, D., Kroeger, T., Straehle, C.N., Kausler, B.X., Haubold, C., Schiegg, M., Ales, J., Beier, T., Rudy, M., et al. (2019). ilastik: interactive machine learning for (bio)image analysis. Nat. Methods *16*, 1226–1232. https://doi.org/10.1038/s41592-019-0582-9.

95. Doench, J.G., Fusi, N., Sullender, M., Hegde, M., Vaimberg, E.W., Donovan, K.F., Smith, I., Tothova, Z., Wilen, C., Orchard, R., et al. (2016). Optimized sgRNA design to maximize activity and minimize off-target effects of CRISPR-Cas9. Nat. Biotechnol. *34*, 184–191. https://doi.org/10.1038/nbt.3437.

96. Sanson, K.R., Hanna, R.E., Hegde, M., Donovan, K.F., Strand, C., Sullender, M.E., Vaimberg, E.W., Goodale, A., Root, D.E., Piccioni, F., and Doench, J.G. (2018). Optimized libraries for CRISPR-Cas9 genetic screens with multiple modalities. Nat. Commun. *9*, 5416. https://doi.org/10.1038/s41467-018-07901-8.

97. NanoString Technologies (2018). nCounter Advanced Analysis 2.0 - User Manual. https://nanostring.com/support-documents/ncounter-advanced-analysis-2-0-user-manual/.

98. Subhash, S., and Kanduri, C. (2016). GeneSCF: a real-time based functional enrichment tool with support for multiple organisms. BMC Bioinf. *17*, 365. https://doi.org/10.1186/s12859-016-1250-z.

99. Dunn, K.W., Kamocka, M.M., and McDonald, J.H. (2011). A practical guide to evaluating colocalization in biological microscopy. Am. J. Physiol. Cell Physiol. *300*, C723–C742. https://doi.org/10.1152/ajpcell.00462.2010.

STAR★METHODS

KEY RESOURCES TABLE

REAGENT or RESOURCE	SOURCE	IDENTIFIER
Antibodies		
APC-Cy7 anti-Human CD25	BD Biosciences	Cat. #557753; RRID:AB_396859
APC anti-Human CD73	Biolegend	Cat. #344006; RRID:AB_1877157
BUV395 anti-Human CD4	BD Biosciences	Cat. #564724; RRID:AB_2738917
BV421 anti-Human CD30	BD Biosciences	Cat. #566253; RRID:AB_2739631
PerCP/Cy5.5 anti-Human CD32	BioLegend	Cat. #303215; RRID:AB_2616924
BV605 anti-Human CD20	BioLegend	Cat. #302333; RRID:AB_11125763
BV510 anti-Human CD2	BioLegend	Cat. #300217; RRID:AB_2566039
PE anti-Human CD279 (PD-1)	BioLegend	Cat. #329905; RRID:AB_940481
BUV737 anti-Human CD49d	BD Biosciences	Cat. #612850;
PE-Cy7 anti-Human CD39	BioLegend	Cat# 328211; RRID:AB_2293623
FITC anti-Human CD98	BioLegend	Cat. #315603; RRID:AB_2190795
BV785 anti-Human CTLA-4	BioLegend	Cat. #369623; RRID:AB_2810581
V450 anti-Human CD69	BD Biosciences	Cat.# 560740; RRID:AB_1727512
Anti-CD73 antibody	Abcam	Cat. #ab175396
Anti-CD3 antibody	Abcam	Cat.# ab11089; RRID:AB_2889189
Alexa 647 anti-rat	ThermoFisher Scientific	Cat. #A21247; RRID:AB_141778
Alexa 647 anti-rabbit	ThermoFisher Scientific	Cat. #A21443; RRID:AB_2535861
Alexa 800 anti-rabbit	ThermoFisher Scientific	Cat. #A32735; RRID:AB_2633284
Streptavidin, Alexa Fluor™ 680 Conjugate	ThermoFisher Scientific	Cat. #S32358
HIV1 p24 antibody	Genetex	Cat. #GTX40774
Anti-p24 primary antibody Monoclonal Anti- HIV-1 p24 Protein, Clone AG3.0	NIH AIDS Reagent Program	Cat. #HRP-20068
Monoclonal Anti-HIV-1 p24 (AG3.0)	NIH AIDS Reagent Program	Cat. #ARP-4121
See Table S1 for a list of CyTOF antibodies		
Bacterial and virus strains		
One Shot Stbl3 Chemically Competent E. coli	ThermoFisher Scientific	Cat. #C737303
Biological samples		
Blood from HIV-seronegative donors	Collected at Vitalant, San Francisco, CA, USA	N/A
Blood from people living with HIV (PLWH) on antiretroviral therapy (ART)	Collected at University of San Francisco, CA, USA	N/A
Tissues from PLWH on ART	Collected at University of Texas, Medical Branch, TX, USA	N/A
Chemicals, peptides, and recombinant proteins		
FseI	New England Biolabs	Cat. #R0588S
AscI	New England Biolabs	Cat. #R0558S
Quick CIP	New England Biolabs	Cat. #M0525S
T4 DNA ligase	New England Biolabs	Cat. #M0202S
Luna Universal qPCR Master Mix	New England Biolabs	Cat. #M3003X
HiScript II Q RT SuperMix for qPCR	Absource Diagnostics	Cat. #R222-01
DMEM	ThermoFisher Scientific	Cat. # 11965-118
RPMI	ThermoFisher Scientific	Cat. #11875-119
Opti-MEM	ThermoFisher Scientific	Cat. #31985062
FBS	Corning	Cat. #35-010-CV

(*Continued on next page*)

Continued

REAGENT or RESOURCE	SOURCE	IDENTIFIER
P/S	Fisher Scientific	Cat. #11548876
Polyethylenimine	Polysciences	Cat. #23966
Fugene HD transfection	Promega	Cat. #E2311
Puromycin	InvivoGen	Cat. #ant-pr-1
SCH-58261	Sigma-Aldrich	Cat. #S4568-5MG
PMA	Sigma-Aldrich	Cat. #10634-1MG
Ionomycin	Sigma-Aldrich	Cat. #10634-1MG
DMSO	Sigma-Aldrich	Cat. #D2650-100ML
Ficoll-Hypaque	Corning	Cat. #25-072-CI
αCD3/αCD28 activating beads	ThermoFisher Scientific	Cat. #11132D
IL-2	PeproTech	Cat. #200-02
DMOG	Sigma-Aldrich	Cat. #D3695
Saquinavir (Protease Inhibitor)	Sigma-Aldrich	Cat. #S8451-50MG
Raltegravir (Integrase Inhibitor)	Sigma-Aldrich	Cat. #CDS023737-25MG
Contaminant-free PBS (for CyTOF experiments)	Rockland	Cat. #MB-008
EDTA (for CyTOF experiments)	Corning	Cat. # 46-034-CI
Barcode Perm buffer	Fluidigm	Cat. # 201057
PFA (for CyTOF experiments)	Electron Microscopy Sciences	Cat. #15700
fix/perm buffer (for CyTOF experiments)	eBioscience, ThermoFisher Scientific	Cat. #88-8824-00
Permeabilization Buffer (for CyTOF experiments)	eBioscience, ThermoFisher Scientific	Cat. #00-8333-56
Cell-ID DNA Intercalator-Ir (for CyTOF experiments)	Fluidigm	Cat. #201192A
Maxpar Cell Staining Buffer (for CyTOF experiments)	Fluidigm	Cat. # 201068
Maxpar PBS (for CyTOF experiments)	Fluidigm	Cat. #201058
Maxpar Cell Acquisition Solution (for CyTOF experiments)	Fluidigm	Cat. #201240
EQ calibration beads (for CyTOF experiments)	Fluidigm	Cat. #201078
retrieval solution	Agilent Dako	Cat. #S1700
Triton X-100	Sigma-Aldrich	Cat. #X100
Zombie viability dye	Biolegend	Cat. #423113
live/dead staining	ThermoFisher Scientific	Cat. #L34961
Prolong Diamond Antifade Mount medium containing DAPI	ThermoFisher Scientific	Cat. #P36931
Cisplatin	Sigma-Aldrich	Cat. #232120-50MG
Critical commercial assays		
NucleoSpin Plasmid, Mini kit	Macherey-Nagel	Cat. #740588
Plasmid Plus Maxi Kit	Qiagen	Cat. #12963
Quick-RNA Miniprep Kit	Zymo Research	Cat. #R1054
HIV-1 alliance p24 ELISA kit	PerkinElmer	Cat. #NEK050001KT
EasySep Human $CD4^+$ T cell Isolation Cocktail	StemCell Technologies	Cat. #17952
luciferase assay system	Promega	Cat. #E2610
nCounter Vantage 3D RNA:Protein Immune Cell Profiling Assay	NanoString Technologies	Cat. #121100019
Cell-ID 20-Plex Pd Barcoding Kit	Fluidigm	Cat. # 201060
PNA ISH kit	Agilent Dako	Cat. #K5201
RNAscope 2.5 HD Detection Reagent-RED	Advanced Cell Diagnostics	Cat. #322360
Deposited data		
NanoString nCounter data, raw and analyzed	This paper	GEO: GSE244193
RNA sequencing data	This paper	GEO: GSE244193

(*Continued on next page*)

Continued

REAGENT or RESOURCE	SOURCE	IDENTIFIER
Experimental models: Cell lines		
Human: HEK293T cells	ATCC	Cat. #CRL-3216
Human: J-Lat 5A8 Cells	Chan et al.[50]	N/A
Human: J-Lat A72 Cells	NIH AIDS Reagent Program	Cat. #ARP-9856
Human: J-Lat 11.1 Cells	Spina et al.[86]	N/A
Human: J-Lat 6.3 Cells	NIH AIDS Reagent Program	Cat. #ARP-9846
Human: JurkatE6	ATCC	Cat. #TIB-152
Human: J-Lat A72 CRISPRi	This paper	N/A
Human: J-Lat A72 CRISPRi CD73KD	This paper	N/A
Human: J-Lat A72 CRISPRi NT	This paper	N/A
Oligonucleotides		
mKO2 DF II + nef FW - AGAA GGCGCGCC ATGGTGAGTGTGATTAAACC	Integrated DNA Technologies	N/A
mKO2 DF II + nef RV - TTCT GGCCGGCC TTAGCTATGAGCTACTGCAT	Integrated DNA Technologies	N/A
dCas9 fw - GGATCGAAGAGGGCATCAAA	Integrated DNA Technologies	N/A
dCas9 rv - GTTCCTGGTCCACGTACATATC	Integrated DNA Technologies	N/A
CD73 fw - CACCGCGTGAACTGGGTGCGAAAG	Integrated DNA Technologies	N/A
CD73 rv - AAACCTTTCGCACCCAGTTCACGC	Integrated DNA Technologies	N/A
NT fw - CACC GTATTACTGATATTGGTGGG	Integrated DNA Technologies	N/A
NT rv - AAAC CCCACCAATATCAGTAATAC	Integrated DNA Technologies	N/A
NEF-PNA Alexa 488 - GCAGCTTCCTCATTGATGG	PNA Bio	N/A
Alu-PNA Cy5 - GCCTCCCAAAGTGCTGGGATTACAG	PNA Bio	N/A
HIV Gag-pol probe	Advanced Cell Diagnostics	Cat. #317691
Recombinant DNA		
1st generation dual reporter virus construct R7GEmC	NIH AIDS Reagent Program	Cat. #ARP-12595
mKO2-N1	Sakaue-Sawano et al.[87]	Addgene, Cat. #54625; RRID:Addgene_54625
HIV-1 dual-tropic envelope (pSVIII-92HT593.1)	NIH AIDS Reagent Program	Cat. #ARP-3077
HIV NL4-3 Luciferase lentiviral vector	Lassen et al.[48]	N/A
lenti-EF1a-dCas9-KRAB-Puro	Ho et al.[88]	Addgene, Cat. #99372; RRID:Addgene_99372
pLKO5.sgRNA.EFS.tRFP	Heckl et al.[89]	Addgene, Cat. #57823; RRID:Addgene_57823
Software and algorithms		
FlowJo software 10.7.1	FlowJo	RRID:SCR_008520
nSolver Analysis Software 4.0	NanoString Technologies	RRID:SCR_023912
Advanced Analysis Software 2.0.115	NanoString Technologies	RRID:SCR_023912
Calculate and draw custom Venn diagrams	Bioinformatics & Evolutionary Genomics[90]	http://bioinformatics.psb.ugent.be/webtools/Venn/
CyTOF software	Fluidigm	RRID:SCR_021055
Cytobank	Beckman Coulter	RRID:SCR_014043
Trimmomatic 0.36	Bolger et al.[91]	RRID:SCR_011848
STAR aligner 2.5.2b	Dobin et al.[92]	RRID:SCR_004463
DESeq2	Love et al.[93]	RRID:SCR_015687
GeneSCF 1.1-p2	Subhash and Kanduri	N/A
Nikon NIS Elements Advanced Research imaging software	Nikon Instruments	RRID:SCR_014329
Ilastik	Berg et al.[94]	RRID:SCR_015246

(*Continued on next page*)

Continued

REAGENT or RESOURCE	SOURCE	IDENTIFIER
GraphPad Prism software version 9	GraphPad Software	RRID:SCR_002798
Cytoscape 3.8.2	Otasek et al.[36]	RRID:SCR_003032
BioRender	BioRender	RRID:SCR_018361
Other		
nCounter SPRINT profiler	NanoString Technologies	RRID:SCR_021712
CyTOF2 instrument	Fluidigm	N/A
LSRII flow cytometer	BD Biosciences	N/A
MA900 Multi-Application Cell Sorter	Sony Biotechnologies	N/A
Cytek Aurora (5L)	Cytek Biosciences	N/A
Ruskinn *Invivo* 400 workstation	Baker	N/A

RESOURCE AVAILABILITY

Lead contact

Further information and requests for resources and reagents should be directed to and will be fulfilled by the lead contact, Satish K. Pillai (satish.pillai@ucsf.edu).

Materials availability

Materials used or generated during this study are available from the lead contact on reasonable request.

Data and code availability

RNA-seq and NanoString data have been deposited at GEO and are publicly available as of the date of publication. Accession numbers are listed in the key resources table. This paper does not report original code. Any additional information required to reanalyze the data reported in this work is available from the lead contact upon request.

EXPERIMENTAL MODEL AND STUDY PARTICIPANT DETAILS

Bacterial strains

One Shot Stbl3 Chemically Competent E. coli (ThermoFisher Scientific) were used for cloning and subsequent generation of large scale cultures for plasmid isolation. Bacteria were grown at 30°C on agar plates in an incubator or in an orbital shaker shaking at 250rpm.

Cell lines

HEK293T cells (ATCC) were cultured in DMEM supplemented with 10% FBS and 1% Penicillin/Streptomycin (DMEM complete = $DMEM^{+/+}$) at 37°C, 5% CO_2 unless stated otherwise. Cells were passaged every 3–4 days when 80% confluent. All J-Lat cell clones were cultured in RPMI 1640 supplemented with 10% FBS and 1% Penicillin/Streptomycin (RPMI complete = $RPMI^{+/+}$) at 37°C, 5% CO_2 unless stated otherwise, and passaged twice per week. J-Lat clone 5A8[50] was kindly provided by Prof. Warner Greene, J-Lat clones A72 and 6.3 received from the NIH AIDS Reagent program and J-Lat 11.1[86] kindly provided Prof. Eric Verdin. Jurkat E6-1 cells were obtained from ATCC. J-Lat A72 CRISPRi and CRISPRi knockdown cells (CD73 KD and NT) were generated in this paper.

Study participants and primary $CD4^+$ T cell culture

This study utilized blood specimens collected from HIV-seronegative individuals (Vitalant) and PLWH enrolled in the University of California, San Francisco (UCSF) SCOPE cohort who were on continuous, suppressive ART for >1 year at time of sampling (see Table S3 for demographic information). Research protocols were approved by the relevant University of California, San Francisco Committees on Human Research. All participants were enrolled after obtaining written informed consent, and all participant data and specimens were coded to protect confidentiality.

First, peripheral blood mononuclear cells (PBMCs) were isolated by Ficoll-Hypaque density gradient centrifugation (Corning) at 2000 rpm (~850 x g) at RT for 30 min, without brake. PBMCs were immediately processed to isolate $CD4^+$ T cells by negative selection using the EasySep Human $CD4^+$ T cell Isolation Cocktail (StemCell Technologies) according to manufacturer's protocol. Purified $CD4^+$ T cells were cultured in $RPMI^{+/+}$ at 37°C, 5% CO_2.

Tissue samples

Tissues from ART-suppressed individuals who have been on treatment for at least 6 months and had viral loads below clinical detection limits (<50 RNA copies/ml), as well as tissues from HIV-negative and ART-naïve viremic individuals with high plasma loads

(>50 RNA copies/ml) were part of an ongoing research protocol approved by University of Texas Medical Branch (UTMB). Further clinical data and additional information are available and will be provided upon request by Dr. Eliseo Eugenin (eleugeni@utmb.edu). All tissues were obtained with full, written consent from the study participants and freshly collected specimens were immediately fixed with 4% PFA, then mounted into paraffin blocks, subjected to tissue sectioning, and ultimately to ab analysis by *in situ* and immunostaining.

METHOD DETAILS

Construction of next generation HIV_{DFII} reporter plasmid

The 1st generation dual reporter virus construct R7GEmC[26] (NIH AIDS Reagent Program) was adapted by ligation-based molecular cloning. Briefly, R7GEmC was linearized by enzymatic digest using FseI and AscI (New England Biolabs) in order to excise the mCherry open reading frame. Then, mKO2 was PCR amplified from the template mKO2-N1[87] (Addgene) using primers containing matching restriction sites. Subsequently, the lentiviral vector was dephosphorylated using Quick CIP, purified and subjected to ligation with the digested and gel-purified PCR product utilizing T4 DNA ligase.

Plasmid amplification and preparation

Circularized plasmid DNA was transformed by heat-shock in One Shot Stbl3 Chemically Competent E. coli for subsequent antibiotics selection and Sanger sequencing (Elim Biopharm) of positive clones.

Transformed Stbl-3 cells were grown in 2–5 mL of lysogeny broth with 0.1 mg/mL Ampicillin (LB Amp) for 16-24h or 4–8 h prior to inoculation of large-volume flask with 100–300 mL LB Amp for overnight growth. 16 h later, cells were pelleted by centrifugation for 15 min at >3000 g and subjected to plasmid preparation using the NucleoSpin Plasmid, Mini kit for plasmid DNA (Macherey-Nagel) or Plasmid Plus Maxi Kits (Qiagen) following the manufacturer's protocol. Concentrations of isolated plasmid DNA was spectrophotometrically determined using a NanoDrop 1000 (ThermoFisher Scientific) and DNA aliquots were stored at 4°C.

Virus production

HIV-1 viruses were generated by transfection of proviral DNA into HEK293T cells via polyethylenimine (PEI, Polysciences) transfection protocol. Env-pseudotyped HIV_{DFII} stocks were produced by co-transfecting plasmids encoding HIV_{DFII} and a plasmid encoding HIV-1 dual-tropic envelope (pSVIII-92HT593.1) at a ratio of 3:1 into HEK293T cells at 50–60% confluency grown in 175 cm^2 culture flasks. Each flask was transfected with a total amount of 30 μg DNA. The transfection mix was prepared in 2 mL Opti-MEM as follows: DNA plasmids were diluted in Opti-MEM first, then PEI was added at a ratio of 3:1 PEI:DNA (90 μg PEI). The transfection mix was vortexed for 15 s and incubated for 15 min at RT. Culture medium was replaced with 20 mL fresh DMEM +10% FBS without P/S, and 2 mL transfection mix was added to each flask. 16h post transfection, P/S-free medium was replaced with standard culture medium ($DMEM^{+/+}$), and cells were incubated for another 24 h at 37°C, 5% CO_2. For replication competent HIV NL4-3 Luciferase,[48] lentiviral vectors were introduced by Fugene HD transfection (Promega) according to the manufacturer protocols. Cell supernatants were collected 48h post transfection, centrifuged at 4°C for 10 min at 4000 rpm (~3390 x g) and subsequently filtered using 0.22 μm membrane vacuum filter units (MilliporeSigma) to remove cell debris. Virus preparations were concentrated by ultracentrifugation at 20,000 rpm (~50,000 x g) for 2h at 4°C and resuspended in complete media for subsequent storage at −80°C. Virus concentration was estimated by p24 titration using the HIV-1 alliance p24 ELISA kit (PerkinElmer).

Generation of CRISPRi cell lines

Stable, knockdown cell lines were generated by lentiviral transduction of dCas9-KRAB, as well as single guide RNAs (sgRNAs). We first generated a CRISPRi cell line by transducing J-Lat A72 with the vector lenti-EF1a-dCas9-KRAB-Puro[88] (Addgene) and subsequent selection with puromycin-containing media (1 μg/mL) for at least one week. Then, J-Lat A72 CRISPRi cells were transduced with the lentiviral vector pLKO5.sgRNA.EFS.tRFP[89] (Addgene), containing target-specific sgRNAs (J-Lat A72 CRISPRi CD73 KD) or a non-targeting control sgRNA (J-Lat A72 CRISPRi NT). SgRNA design was conducted using the CRISPick-tool developed by the Broad Institute[95,96] and sgRNA cloning was performed following the detailed protocol provided by Heckl et al. (2014).[89] All established cell lines were tested by qPCR using specific primers and the Luna Universal qPCR mix (NEB) according to the manufacturer's instructions upon RNA extraction (Zymo Research) and cDNA synthesis (. Primer sequences for qPCR and sgRNA cloning are listed in the key resources table.

J-Lat cell latency reversal

J-Lat 5A8 cells (seeded at $1x10^6$ cells/ml) were incubated with SCH-58261 (Sigma-Aldrich) at 37°C for 1h at increasing doses in $RPMI^{+/+}$, followed by stimulation with 20 nM PMA/1 μM Ionomycin (PMA/I, Sigma-Aldrich). Untreated cells or cells treated with 0.5% DMSO served as negative controls. 7h after PMA/I reactivation, cells were washed 2x with PBS and viral transcriptional activity, reflected by GFP expression was measured using LSR II flow cytometer (BD Biosciences).

Analyses of latency reversal in J-Lat A72 CRISPRi CD73 KD and J-Lat A72 CRISPRi NT included an additional pre-gating for-RFP positive cells to specifically select for KD cells prior to quantification of GFP expression.

CD4+ T cell culture under hypoxic conditions

Following CD4+ T cell isolation, cells were activated with with αCD3/αCD28 activating beads (ThermoFisher Scientific) for 48 h at a concentration of 1 bead/cell in the presence of 100 U/ml IL-2 (PeproTech) in RPMI +/+ and were subsequently cultured under hypoxia (HOX - 1% O_2; Ruskinn *Invivo* 400 workstation), standard conditions (normoxia - NOX - 21% O_2), or were treated with 500 μM DMOG (Sigma-Aldrich) up to 5 days post stimulation.

CD4+ T cell *in vitro* infection

CD4+ T cells were stimulated as described above for 3 days (initial seeding concentration $1x10^6$ cells/ml). At the day of infection, cells were spinoculated in 96-well V-bottom plates (MilliporeSigma) in 50 μL $RPMI^{+/+}$ with 100 ng (HIV_{DFII}) of p24 per 1×10^6 cells with 5×10^6 cells total per well for 2 h at 2350 rpm (1173 × g) at 37°C. After spinoculation, all cells were returned to culture in the presence of 30 U/ml IL-2. Pre-stimulated CD4+ T cells stayed in αCD3/αCD28 activating beads during spininfection and subsequent cell culture. Samples were subjected to further processing 4 days post infection unless stated otherwise.

For experiments mimicking hypoxic conditions, cells were treated with 500 μM DMOG or mock-treated with 0.5% DMSO two days after αCD3/αCD28 bead stimulation and 24h before HIV_{DFII} spininfection. Cells were kept in DMOG containing $RPMI^{+/+}$, in presence of activation beads and IL-2 until sample collection 4 days post infection.

CD4+ T cell *in vitro* infection and latency reversal

Initially, CD4+ T cells were isolated from peripheral blood as described above and subjected to FACS of $CD73^+$ and $CD73^-$cells. To that aim, cells were stained with APC anti-human CD73 (BioLegend) diluted in PBS (1:20) in 100 μL final volume for 20 min at RT. Cells were then washed twice with PBS and resuspended in 500 μL–1000 μL PBS to achieve high cell concentrations (20 - $40x10^6$ cells/ml) for FACS. Cells were sorted into 15 mL conical tubes containing 1.5 mL $RPMI^{+/+}$. Cells were cultured for 24h, then infected and rested in the presence of ART to establish *in vitro* latency.[48] Briefly, 100 ng of purified NL4-3-Luciferase was added per $1x10^5$ sorted cells, which were then infected by spinoculation as described above. 24h post virus exposure, 5 μM saquinavir was added to the cell cultures to suppress spreading infection. 5 days later, cells were stimulated with αCD3/αCD28 beads (or left untreated) in the presence of 30 μM raltegravir to prevent new infections. 24h after stimulation, luciferase activity was quantified using the bright glo luciferase assay system (Promega).

CD4+ T cell staining and processing

CD4+ T cells were stained for viability, using the fixable Zombie viability dye (1:100; BioLegend) according to the manufacturer's protocol. Subsequently, antibodies APC-Cy7 anti-Human CD25 (1:100, BD Biosicences) and V450 anti-Human CD69 (1:100, BD Biosciences), or APC anti-Human CD73 (1:50) diluted in PBS were added for cell surface staining and incubated for 20 min at RT. For flow cytometry, cells were washed and then fixed in 1% paraformaldehyde (PFA) in PBS after the staining. FACS experiments to isolate populations of interest (CD73-/CD73+ cells) were performed with live, unfixed cell samples. Flow cytometry analyses were performed on the LSR II flow cytometer (BD Biosciences) or MA900 Multi-Application Cell Sorter (Sony Biotechnologies). All fluorescent-based sorts were conducted on the latter instrument.

Immunophenotyping of CD4+ T cells from HIV-infected individuals

30 mL of fresh blood were obtained from six HIV-positive individuals on long-term continuous ART (greater than one year) who were stably suppressed (HIV RNA <40 copies/ml); samples were processed as described above. Purified CD4+ T cells were then stained using a panel of antibodies against previously described reservoir markers (see Figure S3), as well as CD4, CD73, CD39 and a live/dead staining (ThermoFisher Scientific). Finally, cells were subjected to flow cytometry measurement on a Cytek Aurora (5L) instrument.

Flow cytometry gating and data analysis

Data were analyzed and visualized using the FlowJo software (v.10.7.1). Crosstalk compensations was performed using single-stained samples for each of the fluorochromes and isotype controls were employed to assess antigen positivity and enable specific gating. FACS and flow cytometry gating was performed as follows: low/negative cells for live/dead dyes were selected for single cells and subsequent FSC/SSC scatterplots. Then, antibody gates were defined based on suited/single stained and isotype controls. Gating of HIV_{DFII} reporter expression was based on non-infected, mock-treated (*in vitro* activated) negative control samples to account for activation-dependent increase of cellular background fluorescence.

Expression profiling via NanoString

Quantitative RNA and protein expression data were generated using the nCounter Vantage 3D RNA:Protein Immune Cell Profiling Assay (NanoString Technologies) and the nCounter SPRINT profiler (NanoString Technologies), comprising 770 RNA and 30 protein targets as well as positive and negative controls. 100,000 viable, sorted cells were used per sample, which were processed according to the manufacturer's instructions. RNA and protein expression values were normalized and analyzed using the nSolver Analysis Software 4.0 and the add-on Advanced Analysis Software 2.0.115 (NanoString Technologies). Samples that did not pass the default control performance and quality parameters were excluded from subsequent analysis. Normalization genes for each sample were

automatically selected by the software based on the geNorm algorithm. Biological replicates were grouped according to sample type and the differential expression of each analyte-type (RNA or protein target) was determined in cross-comparisons among all sample types by considering inter-donor differences as confounding variable unless otherwise stated. Intersections of significant targets of individual differential expression analyses were visualized in a Venn diagram using an open source platform from Bioinformatics & Evolutionary Genomics.[90]

Based on the differential expression of each gene, gene sets pre-defined by nanoString, representing different pathways included in this assay, were analyzed by calculating global significance scores for each gene set within each sample as follows: undirected global significance statistic = $\left(\frac{1}{p}\sum_{i=1}^{p} t_i^2\right)^{\frac{1}{2}}$, where ti is the t-statistic from the ith pathway gene. The directed global significance statistic is similar to the undirected global significance statistic, but rather than measuring the tendency of a pathway to have differentially expressed genes, it measures the tendency to have over- or under-expressed genes. It is calculated similarly to the undirected global significance score, but it takes the sign of the t-statistics into account: Directed global significance statistic = $sign(U)|U|^{1/2}$ where U = $\left(\frac{1}{p}\sum_{i=1}^{p} sign(t_i) * t_i^2\right)$ and where sign(U) equals −1 if U is negative and 1 if U is positive.[97]

CyTOF samples preparation and analysis

For live/dead discrimination, 0.1–1 million cells per sample were treated with cisplatin (Sigma-Aldrich) and fixed with PFA as previously described.[9,28,29] Briefly, Cells were washed once with contaminant-free PBS (Rockland) with 2 mM EDTA (Corning), centrifuged and resuspend with 25 μM cisplatin in 4 mL PBS/EDTA and incubated for 60 s at room temperature, and then quenched with CyFACS (metal contaminant-free PBS supplemented with 0.1% bovine serum albumin and 0.1% sodium azide). Cells were then centrifuged, fixed with 2% PFA (Electron Microscopy Sciences) in metal contaminant-free PBS and washed 3x with CyFACS. These fixed cells were stored at −80°C until CyTOF staining.

Prior to CyTOF staining, multiple samples were barcoded using the Cell-ID 20-Plex Pd Barcoding Kit according to manufacturer's instructions (Fluidigm). Briefly, each sample was washed twice with Barcode Perm buffer (Fluidigm), and incubated for 30 min with the appropriate barcode at a 1:90 ratio. Cells were then washed with 0.8 mL Maxpar Cell Staining buffer (Fluidigm) in Nunc 96 Deep-Well polystyrene plates (Thermo Fisher), followed by CyFACS. Barcoded samples were combined and blocked with sera from mouse (Thermo Fisher), rat (Thermo Fisher), and human (AB serum, Sigma-Aldrich) for 15 min at 4°C. Cells were washed twice with CyFACS buffer and stained with the cocktail of CyTOF surface staining antibodies (Table S1) for 45 min on ice. Subsequently, cells were washed 3X with CyFACS buffer and fixed overnight at 4°C with 2% PFA in metal contaminant-free PBS. For intracellular staining, cells were permeabilized by incubation with fix/perm buffer (eBioscience) for 30 min at 4°C and washed twice with Permeabilization Buffer (eBioscience). Cells were blocked again with sera from mouse and rat for 15 min on ice, washed twice with Permeabilization Buffer, and stained with the cocktail of CyTOF intracellular staining antibodies (Table S1) for 45 min on ice. Cells were then washed once with CyFACS and incubated for 20 min at room temperature with 250 nM Cell-ID DNA Intercalator-Ir (Fluidigm) in 2% PFA diluted in PBS. Cells were washed twice with CyFACS, once with Maxpar Cell Staining Buffer (Fluidigm), once with Maxpar PBS (Fluidigm), and once with Maxpar Cell Acquisition Solution (CAS, Fluidigm). Immediately prior to acquisition, cells were resuspended in EQTM calibration beads (Fluidigm) diluted in CAS. Cells were acquired at a rate of 250–350 events/sec on a CyTOF2 instrument (Fluidigm) at the UCSF Parnassus single cell analysis facility.

Data were normalized to EQTM calibration beads and de-barcoded with CyTOF software (Fluidigm). Normalized data were imported into FlowJo (BD) for gating (cell, intact, live, single events) and heatmaps were generated in Cytobank upon quality control check.

RNA sequencing

Freshly isolated $CD4^+$ T cells from healthy blood donors were sorted based on their CD73 expression. $3x10^6$ $CD73^-$and $CD73^+$ $CD4^+$ T cells were collected respectively, and stored as dry cell pellets at −80°C. RNA preparation, library preparation and mRNA sequencing were conducted at Genewiz (USA). Paired-end sequencing was performed using the Illumina NovaSeq 6000 instrument to obtain a minimum of 20 million read pairs per sample with a read length of 2x150 bp. Sequence reads were trimmed to remove possible adapter sequences and nucleotides with poor quality using Trimmomatic v.0.36.[91] The trimmed reads were mapped to the Homo sapiens GRCh38 reference genome available on ENSEMBL using the STAR aligner v.2.5.2b.[92] Unique gene hit counts were calculated by using featureCounts from the Subread package v.1.5.2. The hit counts were summarized and reported using the gene_id feature in the annotation file. Only unique reads that fell within exon regions were counted. After extraction of gene hit counts, the gene hit counts table was used for downstream differential expression analysis. Using DESeq2,[93] a comparison of gene expression between samples was performed adjusting for the donor effect as confounding variable. The Wald test was used to generate p values and $\log_2$ fold changes. Genes with an adjusted p value <0.05 (Benjamini-Hochberg method) and absolute $\log_2$ fold change >1 were called as differentially expressed genes for each comparison. A gene ontology analysis was performed on the statistically significant set of genes by implementing the software GeneSCF v.1.1-p2.[98] The goa_human GO list was used to cluster the set of genes based on their biological processes and determine their statistical significance. A list of genes clustered based on their gene ontologies was generated.

In situ detection of HIV and cellular markers in tissue samples

The experimental procedure for the *in situ* and immunofluorescence staining has been described in detail in previous publications.[53,54] The assay enables the detection of HIV-integrated DNA, viral mRNA, viral proteins, and several cellular markers in the same assay. Sample preparation, data acquisition and subsequent analyses were conducted in the laboratory of Dr. Eliseo Eugenin (UTMB, Texas). Briefly, the procedure was performed as follows: Paraffin-embedded slides containing the tissue samples were consecutively immersed in the following solutions: xylene for 5 min (2 times), 100% EtOH for 3 min, 100% EtOH for 3 min, 95% EtOH for 3 min, 90% EtOH for 3 min, 70% EtOH for 3 min, 60% EtOH for 3 min, 50% EtOH for 3 min, miliQ H_2O for 3 min. Then, tissue was encircled with ImmEdge Pen to reduce the reagent volume needed to cover the specimens. Finally, slides were immersed in miliQ H_2O for 3 min. For Protein K treatment, tissues were incubated with proteinase K diluted 1:10 in 1X TBS (Fisher Scientific; and PNA ISH kit, Agilent Dako) for 10 min at RT in a humidity chamber. Next, slides were immersed in miliQ H2O for 3 min, then immersed in 95% EtOH for 20 s and finally, the slides were left air-dry for 5 min. For HIV DNA probe hybridization tissues were incubated with 10 μM PNA DNA probe for Nef-PNA Alexa Fluor 488 and Alu-PNA Cy5 (PNA Bio). Next, slides were placed in a pre-warmed humidity chamber and incubated at 42°C for 30 min, then the temperature was raised to 55°C for an additional 1 h incubation. Subsequently, tissues were incubated using Preheat Stringent Wash working solution (PNA ISH kit) diluted 1:60 in 1X TBS for 25 min in an orbital shaker at 55°C. Slides were equilibrated to RT by brief immersion in TBS for 20 s. HIV mRNA detection followed the manufacturer's protocol for RNAscope 2.5 HD Detection Reagent-RED (Advanced Cell Diagnostics). Probe for HIV Gag-pol was added to the tissue samples and incubated for 30 min at 42°C and then 50 min at 55°C. Next, samples were incubated in Preheat Stringent Wash working solution diluted 1:60 in 1X TBS (PNA ISH kit) for 15 min in an orbital shaker at 55°C. Finally, slides were immersed in 1X TBS for 20 s. For HIV or cellular protein detection, antigen retrieval was performed by incubating slide sections in commercial antigen retrieval solution (Agilent Dako) for 30 min in a water-bath at 80°C. Next, slides were removed from the bath and cooled down in 1X TBS. Samples were permeabilized with 0.1% Triton X-100 (Sigma-Aldrich) for 2 min and then washed in 1X TBS for 5 min three times. Unspecific antibody binding sites were blocked by incubating samples with a freshly prepared blocking solution. Afterward, sections were incubated overnight at 4°C using a humidity chamber (10 mL of blocking solution: 1 mL 0.5 M EDTA, 100 μl Fish Gelatin from cold water 45%, 0.1 g Albumin from Bovine serum Fraction V, 100 μl horse serum, 5% human serum, 9 mL miliQ H_2O). Anti-p24 primary antibodies were added to the samples diluted in a blocking solution and incubated at 4°C overnight. To perform these analyses, large amounts of antibodies (obtained from the NIH AIDS repository) were purified and pre-absorbed in uninfected human tissues as well as tested in cell lines to assure specificity and proper binding to the target (see Donoso et al.[53] for details). Following antibody staining, slides were washed in 1X TBS 5 min for three times to eliminate unbound antibodies. Secondary antibodies were added at the appropriate dilutions and incubated for 2h at RT. Slides were washed three times in 1X TBS for 5 min to eliminate unbound antibodies. Next, slides were mounted using Prolong Diamond Antifade Mount medium containing DAPI (ThermoFisher Scientific). Slides were kept in the dark at 4°C.

Image acquisition and analysis

Cells were examined by confocal microscopy using an A1 Nikon confocal microscope with spectral detection and unmixing systems. Image analysis was performed using the Nikon NIS Elements Advanced Research imaging software (Nikon Instruments). The automated image segmentation and analysis are based on the following premises: For detection of HIV-integrated DNA, first, automatic or manual detection of cells that are positive for HIV-DNA and second, the HIV-DNA probe has to colocalize with DAPI and Alu repeats staining with a Pearson's correlation coefficient of at least 0.8 as described previously.[99] These two conditions are essential for HIV-integrated DNA, or the signal is considered negative or unspecific. For detection of HIV-mRNA, first, low colocalization with DAPI or Alu-repeats (0.2 Pearson's correlation coefficient or below) and second, presence in cells with HIV-DNA signal. The sensitivity, accuracy and specificity of the system were previously validated in the laboratory of our collaborator in two well characterized T cell lines A3.01 (uninfected) and ACH-2 (HIV-infected) and two monocytic cell lines, HL-60 (uninfected) and OM-10 (HIV-infected).

To analyze local microenvironments of $CD3^+$ cells, CD73 expression was assessed in cell neighborhoods by lineplot analysis. Image segmentation and quantification were performed using Nikon NIS Elements Advanced Research imaging software and Ilastik.[94] CD73 signals were analyzed along straight lines of 80 μM length, placing the zero point at the center of the line, at the position of the respective CD3-positive cell. Obtained CD73 intensities were normalized to the mean CD73 intensity in $CD3^+$ HIV-DNA-/p24+ (ART suppr.) samples (see Figure S7).

QUANTIFICATION AND STATISTICAL ANALYSIS

Statistical details are given in the figure legends. All statistical analyses were performed using GraphPad Prism software version 9. p-values ≤ 0.05 were considered statistically significant. A Student's two-tailed t test was used for two-way column analyses. ANOVA tests were used for multiple comparisons. p-values are denoted in the figure panels. Data are presented as means with error bars indicating the standard error of the mean (SEM) unless otherwise stated.